Dynamical Processes on Metric Networks*

Lucas Böttcher[†] and Mason A. Porter[‡]

Abstract. The structure of a network has a major effect on dynamical processes on that network. Many studies of the interplay between network structure and dynamics have focused on models of phenomena such as disease spread, opinion formation and changes, coupled oscillators, and random walks that one can describe using coupled ordinary differential equations, difference equations, stochastic processes, or agent-based models. In parallel to these developments, there have been many studies of wave propagation and other spatially extended processes on networks. These latter studies consider metric networks, in which the edges are associated with real intervals. Metric networks give a mathematical framework to describe dynamical processes that include both temporal and spatial evolution of some quantity of interest — such as the concentration of a diffusing substance or the amplitude of a wave — by using edge-specific intervals that quantify distance information between a network's nodes. Dynamical processes on metric networks often take the form of partial differential equations (PDEs). In this paper, we present a collection of techniques and paradigmatic linear PDEs that are insightful for analyzing the interplay between structure and dynamics in metric networks. We start by considering a time-independent Schrödinger equation. We then use both finite-difference and spectral approaches to study the Poisson, heat, and wave equations as paradigmatic examples of elliptic, parabolic, and hyperbolic PDEs on metric networks. In our numerical experiments, we consider metric networks with up to about 10^4 nodes and 10^4 edges. Additionally, using our spectral approach, we are able to resolve degenerate eigenmodes. A key contribution of our paper is to increase the accessibility of studying PDEs on metric networks. Software that implements our numerical approaches is available at https://gitlab.com/ComputationalScience/metric-networks.

Key words. networks, metric graphs, quantum graphs, partial differential equations, dynamical systems on networks, spatially extended systems

MSC codes. 05C82, 35R02, 81P45

DOI. 10.1137/24M1628153

1. Introduction. The study of dynamical processes on networks has led to many insights into the interplay between network structure and dynamics [67, 80, 129, 143, 154]. For example, in models of disease spread [39, 149], opinion dynamics [72, 170], and coupled oscillators [113, 156], researchers have derived conditions for bifurcations and phase transitions between qualitatively different behaviors. These results have often been accompanied by in-

^{*}Received by the editors January 1, 2024; accepted for publication (in revised form) by J. Bronski April 12, 2025; published electronically October 17, 2025.

https://doi.org/10.1137/24M1628153

Funding: The work of the first author was supported by hessian.Al and the Army Research Office grant W911NF-23-1-0129.

[†]Department of Computational Science and Philosophy, Frankfurt School of Finance and Management, 60322 Frankfurt, am Main, Germany and Department of Medicine, University of Florida, Gainesville, FL 32610 USA (l.boettcher@fs.de).

[‡]Department of Mathematics, University of California, Los Angeles, CA 90095 USA; Department of Sociology, University of California, Los Angeles, CA 90095 USA; Santa Fe Institute, Santa Fe, NM 87501 USA (mason@math.ucla.edu).

sights into the effectiveness of specific interventions and how various types of failures affect the robustness of structures such as communication networks [3, 50, 51, 83, 128], heterogeneous materials [26, 33, 155], and social networks [54, 55, 161, 177]. In these applications, it is common for dynamical processes on networks to take the form of ordinary differential equations (ODEs), with each node of a network associated with one or more ODEs, which describe how the nodes' states evolve. It is also common for dynamical processes on networks to take the form of difference equations, stochastic processes, and agent-based models.

In parallel to these studies, there has also been a wealth of research on metric networks 120, 121, 124, 125, 132, 153, 162, 164]. A metric network consists of a combinatorial graph $\mathcal{G} = (\mathcal{V}, \mathcal{E})$ along with a metric to measure distances along the edges of the graph. Each edge $(u,v) \in \mathcal{E}$, which connects the nodes $u,v \in \mathcal{V}$, is associated with a real interval $[0,\ell_{uv}]$ of length ℓ_{uv} . If we explicitly know the position \mathbf{x}_u of each node $u \in \mathcal{V}$, then $\ell_{uv} = \|\mathbf{x}_u - \mathbf{x}_v\|$ for a suitable norm $\|\cdot\|$, such as the Euclidean norm or (more generally) a p-norm. Metric networks encompass a wide variety of networked systems in which distance information between nodes is necessary to mathematically describe corresponding physical, chemical, or biological processes. Because of the edge-specific intervals $[0, \ell_{uv}]$, one can equip a metric network with a differential operator, rather than a discrete operator (such as the combinatorial graph Laplacian), which one employs in studies of combinatorial networks (i.e., the usual type of network). One can thereby study partial differential equations (PDEs) on networks. There are also some papers that study PDEs, such as reaction-diffusion systems, on combinatorial networks (e.g., see [10, 11]). Another relevant research thrust is the study of PDEs on graphons (see, e.g., [131]), which one can obtain in appropriate limiting situations from combinatorial networks.

For additional information about metric networks, see the book chapter [20] and the books [22, 115].

1.1. Prior research on metric networks and related systems. In Table 1, we overview a variety of models and application areas in the study of metric networks. Given the wide range of scientific domains in which PDEs on metric networks arise, we mention only a small portion of the available literature. For another summary of application areas, see Chapter 7 of [22].

As an illustration, consider a mass–spring network. In such a network, each node u is a mass and each edge (u,v) is a spring. The end points of (u,v) are nodes with positions x_u and x_v , which we assume for simplicity are located on a line. This example does not yield a PDE on a network, but it enables us to (1) motivate the use of edge-specific length intervals in metric networks and (2) establish connections between metric networks and combinatorial networks. Mass–spring networks are common in models of engineering and material structures [9, 19, 38, 85, 87, 90, 94] and in computer graphics [142, 167]. Such networks have also inspired the development of the Gaussian-network model [15, 53, 86] and anisotropic-network model [12, 65] of macromolecules.

¹We use the term "metric network" instead of "metric graph" to strengthen the link between our work and the network-science literature, where the term "network" is much more common than the word "graph" and also sometimes refers to more general objects than ordinary graphs. Given the rich tradition of studying Schrödinger operators on metric networks, some researchers (see, e.g., [22, 111, 112]) specifically use the term "quantum graph".

 Table 1

 Several models and application areas of metric networks.

Model	Comments	References [4, 20, 22, 103, 104, 110, 111, 112, 157] [5, 28, 46, 47, 123, 136, 137, 138, 139, 140, 150, 166]	
Quantum graphs	Models of quantum dynamics in thin structures.		
Transmission-line and electrical networks	Such networks consist of resistance, inductance, capacitance, and conductance elements.		
Beam networks	Models of beam structures in solid mechanics ($e.g.$, in civil engineering).	[21, 61, 116, 133]	
Traffic flow on networks	Flow models of vehicular and pedestrian traffic, telecommunication networks, and supply chains.	[56, 88, 151]	
Gas networks	Distribution networks that consist of pipes, valves, compressors, and heating and cooling elements.	[17, 43, 63, 64, 134]	

In our example mass–spring network, the length of the edge (u, v) is $\ell_{uv} = |x_u - x_v|$. Let w_{uv} denote the corresponding spring constant. By Hooke's law, the force that is exerted at node u in the direction of node v is $w_{uv}(x_v - x_u)$, which is proportional to ℓ_{uv} [75]. We fix a subset $W \subseteq V$ of the nodes at certain points in space and seek to determine the equilibrium positions of the remaining nodes, which constitute the complementary subset $V \setminus W$. At equilibrium, the mass–spring network is at a minimum of its potential energy $\sum_{(u,v)\in\mathcal{E}} w_{uv}(x_u - x_v)^2/2 = \sum_{u,v} x_u x_v L_{uv}$, where L_{uv} denotes entry (u,v) of the matrix L and we note that $w_{uv} = w_{vu}$. The matrix L, which has entries $L_{uv} = -w_{uv}$ for $u \neq v$ and $L_{uu} = \sum_{v \neq u} w_{uv}$, is the combinatorial graph Laplacian [143]. For nodes $u \in V \setminus W$, one achieves this minimum when

(1.1)
$$\sum_{\{v: (u,v) \in \mathcal{E}\}} w_{uv}(x_u - x_v) = \sum_{\{v: (u,v) \in \mathcal{E}\}} x_v L_{uv} = 0.$$

The lengths ℓ_{uv} in our spring-system example of a metric network are the equilibrium distances that allow all spring forces to balance each other.

The early focus of research on metric networks concentrated predominantly on Schrödinger equations on networks. The linear Schrödinger equation plays a central role in studies of quantum graphs, in which one uses metric graphs and considers quantum dynamics in thin structures [4, 20, 22, 103, 104, 110, 111, 112, 157]. One can also incorporate a cubic nonlinearity to obtain a cubic nonlinear Schrödinger (NLS) equation, which is a paradigmatic system with diverse applications. It arises via a mean-field description of Bose–Einstein condensates [152], as an envelope equation in optics [126], and in many other situations. In the context of metric networks, cubic NLS equations have been considered on a Y-junction and on tree and triangle networks that are built from Y-junctions [144], on a dumbbell network [127], and on a star network [97]. Other studies of nonlinear PDEs on metric networks include examinations of a nonlinear Dirac equation (a relativistic wave equation) on a Y-junction [158], the sine-Gordon equation on star and tree networks [163], the Korteweg–de Vries equation on a star network [45], and reaction–diffusion equations [174].

Metric networks also arise in the mathematical description of transmission-line and electrical networks. Such networks are usually described by lumped-element models with resistance, inductance, capacitance, and conductance elements arranged in a network, through which signals can propagate [5, 47, 136, 137, 138, 139, 140, 150, 166]. For example, in Sections 22.6 and 22.7 of [70], Feynman et al. used an infinite ladder network that consists of capacitors and inductors to illustrate the function of a low-pass filter that prevents the propagation of high-frequency modes of electromagnetic waves. In linear transmission lines, the propagation of electromagnetic waves is described by the telegraph equation [150]. Due to the mathematical similarities between the telegraph equation and Schrödinger systems on metric networks, quantum graphs have been studied experimentally using transmission-line and waveguide networks [28, 46, 62, 95, 118, 123, 181].

Metric networks also appear prominently in other applications. For example, in civil engineering, metric networks arise in the context of beam structures, which are described by 4th-order PDEs [21, 61, 116, 133]. Additionally, networks of resistors have been used to model composite materials that consist of a combination of conducting and nonconducting materials [60, 89, 101, 179]. In quantum communication networks [145], information is transmitted through metric networks (e.g., through optical fibers). It is also common to employ metric networks in studies of transport processes, including the flow of traffic, supplies, and gas in infrastructure and distribution networks [17, 43, 56, 63, 64, 88, 134, 135, 151].

There are also related dynamical processes that are spatially extended and often arise through discretizations of PDEs. Examples of such dynamical processes include nonlinear lattice systems [48, 71, 98, 99, 106] and coupled-oscillator networks that yield classical analogues of topological insulators [160, 168] and spin-orbit coupling [159]. The Ablowitz-Ladik model [1, 2, 176] is a network of nonlinear elements that arises by discretizing an NLS equation. Other nonlinear lattice models, which are also relevant to study on more general network structures, include Fermi-Pasta-Ulam-Tsingou (FPUT) lattices [57, 69, 73, 74, 84, 122] and Toda lattices [169, 171, 172, 173].

1.2. Our contributions. Most existing studies of PDEs on metric networks have focused on very small networks [153]. It is challenging to develop robust numerical methods to solve different types of PDEs and account for diverse boundary conditions on metric networks. The discretization of PDEs can yield large systems of equations that are difficult to handle numerically, especially for metric networks with many edges and PDEs that require a very small step size for numerical integration. Alternatively, one can employ spectral methods, although it is also challenging to identify characteristic wavenumbers and corresponding eigenmodes² with high numerical precision.

In the present paper, we study Poisson, heat, and wave equations as paradigmatic examples of linear elliptic, parabolic, and hyperbolic PDEs on metric networks. Building on previous work [8, 42, 78, 108], we present different simulation approaches that are useful to study such linear PDEs on metric networks. Specifically, we generalize the spectral approach in [42, 78] to account for degenerate eigenmodes. Complementing the numerical results by

²In the present paper, because we often study wave phenomena, we frequently use the term "eigenmode" instead of "eigenfunction" to emphasize the interpretation of eigenfunctions as normal modes in a metric network.

Brio et al. [42], who examined the Poisson equation and the telegraph equation on a metric network with 3 edges, we study the Poisson equation, heat equation, and wave equation on three different metric networks. Our numerical computations use sparse-matrix representations, which allow us to study metric networks with up to about 10⁴ nodes and about 10⁴ edges. Elliptic and parabolic PDEs have been studied on networks of similar sizes using a finite-element method [8]. A key contribution of our paper is to increase the accessibility of studying PDEs on metric networks.

Other software packages have also been developed recently for simulating PDEs on metric networks. The GraFiDi library [27] (which is available at https://plmlab.math.cnrs.fr/cbesse/grafidi) allows one to simulate nonlinear PDEs on metric networks in Python, and QGLAB [82] (which is available at https://github.com/manroygood/Quantum-Graphs) is a MATLAB library for both linear and nonlinear PDEs on metric networks. Both software packages, which were illustrated using the cubic NLS equation as a focal example, employ a finite-difference approach. QGLAB also provides users with the option to select Chebyshev collocation as an alternative discretization method.

- 1.3. Organization of our paper. Our paper proceeds as follows. In Section 2, we define metric networks and discuss common boundary conditions in the study of PDEs on metric networks. We also present an illustrative example with a Schrödinger operator on a two-node network. In Section 3, we overview numerical and analytical methods that are useful to study metric networks. In Section 4, as another elucidatory example, we consider the Schrödinger equation on a star network, where symmetries lead to eigenmode degeneracies. In Section 5, we study Poisson, heat, and wave equations on metric networks. In Section 6, we summarize and discuss our results. In Appendix A, we discuss group-theoretic methods that can help identify degenerate eigenmodes in metric networks.³ In Appendix B, we numerically solve the Poisson equation on metric networks with up to about 10⁴ nodes and about 10⁴ edges. On an i7 CPU core with a 1.8 GHz clock speed, the computation for the roughly 10,000-edge network takes about 1.2 hours. Our code for our numerical simulations is available at https://gitlab.com/ComputationalScience/metric-networks.
- 2. Metric networks. In Section 2.1, we present some basic definitions and concepts for studying metric networks. In Sections 2.2 and 2.3, we overview different operators and boundary conditions in the study of PDEs on metric networks. As an illustrative example, in Section 2.4, we solve the Schrödinger equation on a 2-node network and show that certain solutions (with appropriate boundary conditions) correspond to the quantum states of a particle in an infinite square well.
- **2.1. Basic definitions and concepts.** Consider a network in the form of a graph $\mathcal{G} = (\mathcal{V}, \mathcal{E})$, where \mathcal{V} is a set of nodes and \mathcal{E} is a set of edges. We use $N = |\mathcal{V}|$ to denote the number of nodes and $M = |\mathcal{E}|$ to denote the number of edges. In a metric network, each edge $(u, v) \in \mathcal{E}$ that connects two nodes $u, v \in \mathcal{V}$ is parameterized by an interval $[0, \ell_{uv}]$ with $0 < \ell_{uv} < \infty$. (Some authors also account for infinite-length edges [111].) This turns the combinatorial graph \mathcal{G} (which, in other contexts, is often called simply a "graph" [143]) into a topological and metric structure. We allow loops (i.e., self-edges) and multiple edges (i.e., multi-edges) between the same nodes. The length of a walk that is associated with edges

 $^{^{3}}$ The wavenumbers of such degenerate eigenmodes have algebraic multiplicities that are larger than 1.

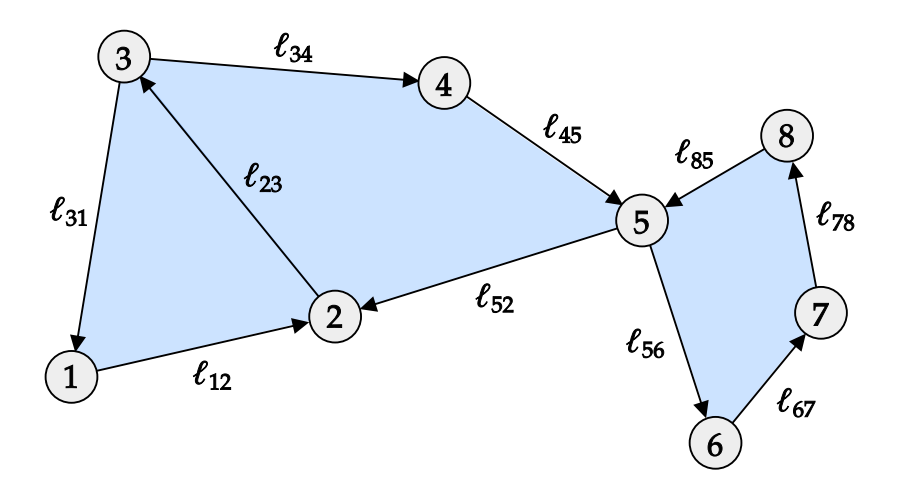


Figure 1. An example of a metric network with N=8 nodes and M=10 edges. The length of an edge that connects two nodes u and v is ℓ_{uv} . The arrows indicate the starting and ending points of an interval. For example, the edge that connects nodes 1 and 2 starts at node 1 and ends at node 2. The depicted metric network is embedded in \mathbb{R}^2 , so each node is associated with a location in the plane. The blue regions indicate polygons whose vertices correspond to the nodes. The edges of these polygons correspond to the intervals (but without their directions).

 $\mathcal{E}' \subseteq \mathcal{E}$ is $\sum_{(u,v)\in\mathcal{E}'}\ell_{uv}$. For example, for the metric network in Figure 1, the length of the walk $1 \to 2 \to 3 \to 4$ is $\ell_{12} + \ell_{23} + \ell_{34}$. In addition to intervals $[0,\ell_{uv}]$, one can equip edges with weights w_{uv} , as we did in the example of mass–spring networks (see Section 1.1), where the weights encode spring stiffnesses. In some applications, it is useful to consider time-dependent edge lengths $\ell_{uv}(t)$ [25].

Metric networks do not have to be embedded in Euclidean space. However, several of the applications in Section 1.1 and Table 1 naturally require such an embedding (e.g., gas networks, transmission lines, and quantum dynamics in thin structures) in real physical implementations of them. One can interpret a metric network as a one-dimensional simplicial complex that consists of one-dimensional simplices (i.e., edges). A key difference between simplicial complexes in combinatorial networks [30] and those in metric networks is that the latter are geometric entities that include length information.

Because of the interval information, a metric network includes all intermediate points on the edges that connect its nodes. This allows us to associate an L^2 space $L^2(\mathcal{G}) := \bigoplus_{(u,v) \in \mathcal{E}} L^2((u,v))$ with a metric network \mathcal{G} . Each edge (u,v) has an associated continuous function $f_{(u,v)} : [0,\ell_{uv}] \to \mathbb{R}$ that maps $x \in [0,\ell_{uv}]$ to the real numbers. We define a function f on a metric network through a collection $\{f_{(u,v)}\}_{(u,v)\in\mathcal{E}}$ of functions, and we require f to be square-integrable. That is,

(2.1)
$$||f||_{L^{2}(\mathcal{G})}^{2} := \sum_{(u,v)\in\mathcal{E}} ||f_{(u,v)}||_{L^{2}((u,v))}^{2} < \infty,$$

where

(2.2)
$$||f_{(u,v)}||_{L^2((u,v))}^2 := \langle f_{(u,v)}, f_{(u,v)} \rangle_{L^2((u,v))} = \int_0^{\ell_{uv}} f_{(u,v)}^2(x) \, \mathrm{d}x \,.$$

We calculate inner products between two functions $f, g \in L^2(\mathcal{G})$ by computing

$$(2.3) \qquad \langle f, g \rangle_{L^{2}(\mathcal{G})} := \sum_{(u,v) \in \mathcal{E}} \langle f_{(u,v)}, g_{(u,v)} \rangle_{L^{2}((u,v))} = \sum_{(u,v) \in \mathcal{E}} \int_{0}^{\ell_{uv}} f_{(u,v)}(x) g_{(u,v)}(x) dx.$$

2.2. Operators. Because of the edge-specific intervals $[0, \ell_{uv}]$, one can equip a metric network with differential operators rather than discrete operators (such as the combinatorial Laplacian), which are studied often in combinatorial networks.

Relevant operators $\mathcal{H}: H^2([0,\ell_{uv}]) \to H^2([0,\ell_{uv}])$ that act on $f_{(u,v)}$ include the negative second derivative

(2.4)
$$\mathcal{H}(f_{(u,v)})(x) = -\frac{\mathrm{d}^2}{\mathrm{d}x^2} f_{(u,v)}(x),$$

the Schrödinger operator

(2.5)
$$\mathcal{H}(f_{(u,v)})(x) = -\frac{\mathrm{d}^2}{\mathrm{d}x^2} f_{(u,v)}(x) + U(x) f_{(u,v)}(x) ,$$

and the magnetic Schrödinger operator [13]

(2.6)
$$\mathcal{H}(f_{(u,v)})(x) = \left(-i\frac{d}{dx} - A(x)\right)^2 f_{(u,v)}(x) + U(x)f_{(u,v)}(x),$$

where $U: [0, \ell_{uv}] \to \mathbb{R}$ is a scalar potential function and $A: [0, \ell_{uv}] \to \mathbb{R}$ is a vector potential function. The space $H^2([0, \ell_{uv}])$ is the Sobolev space of twice-differentiable functions on the interval $[0, \ell_{uv}]$. Sobolev spaces arise commonly in the analysis (including numerical analysis) of PDE problems in their weak formulations [68]. For a metric network with edges $(u, v) \in \mathcal{E}$, the function space is $\bigoplus_{(u,v)\in\mathcal{E}} H^2([0,\ell_{uv}])$.

2.3. Boundary conditions. To solve a PDE on a metric network, we need suitable boundary conditions at the end points $x \in \{0, \ell_{uv}\}$ of all functions $f_{(u,v)}(x)$. We first require that the function f, which is defined by the collection $\{f_{(u,v)}\}_{(u,v)\in\mathcal{E}}$ of functions, satisfies a continuity condition on \mathcal{G} . That is, for each node u with degree $\deg(u)$, the function f needs to satisfy $\deg(u) - 1$ equations that ensure the continuity of all $\deg(u)$ functions $f_{(u,v)}(x)$. Additionally, for each node u, it is common to employ the Kirchhoff flux condition

(2.7)
$$\sum_{e \in \mathcal{E}_{r}} \frac{\mathrm{d}f_{e}(x)}{\mathrm{d}x} \bigg|_{x=x_{e}^{*}} = 0,$$

where \mathcal{E}_u denotes the set of edges that are attached to node u and the quantity x_e^* , where $e \in \mathcal{E}_u$ is an edge, denotes the coordinate of node u at which we evaluate the derivative of $f_e(\cdot)$. As in [20, 111], we use the convention of taking derivatives away from a node into an edge. Some researchers refer to the Kirchhoff condition as the "Kirchhoff–Neumann" condition or the "Neumann" condition (see, e.g., [20, 111]). The connection to the Neumann condition in standard PDE problems becomes apparent if we consider a node u with a single incident edge e. In this case, Eq. (2.7) requires that the derivative of $f_e(\cdot)$ vanishes at the node u.

Let \mathcal{H} denote the operator that includes both the relevant derivatives and the boundary conditions on \mathcal{G} . In the present paper, we focus on PDE problems that involve negative

second derivatives of $f_{(u,v)}(x)$ with respect to x [see Eq. (2.4)] and primarily consider the Kirchhoff flux condition (2.7). It has been shown [22, 102, 111] that the resulting operator $\widetilde{\mathcal{H}} = -\widetilde{\Delta}$ (the generalized negative Laplacian operator that includes continuity conditions and boundary conditions at all nodes) is self-adjoint and hence has an orthonormal eigenbasis and real eigenvalues. This is a key result in the study of metric networks, as it allows one to expand PDE solutions in the eigenbasis of $\widetilde{\mathcal{H}}$.

Another boundary condition that preservers the self-adjointness of the Schrödinger operator (2.4) is the Dirichlet condition

(2.8)
$$f_e(x)|_{x=x_s^*} = 0 \quad \text{for all} \quad e \in \mathcal{E}_u.$$

Imposing Dirichlet conditions at each node yields a metric network that consists of noninteracting edges.

In the present paper, we use the term "coupling conditions" to refer to the combination of continuity conditions and (either Kirchhoff or Dirichlet) boundary conditions for all nodes.

2.4. Two-node system. As an illuminating example, we examine a PDE on a simple metric network. Consider the linear, time-independent Schrödinger equation on a 2-node network with a single edge of length ℓ . We seek to solve the Schrödinger (*i.e.*, Helmholtz) equation

(2.9)
$$\frac{\mathrm{d}^2 f(x)}{\mathrm{d}x^2} = -k^2 f(x), \quad x \in [0, \ell].$$

When we use the Kirchhoff flux condition (2.7) for the boundary conditions, we have f'(0) = 0 and $-f'(\ell) = 0$. For completeness (and pedantry), we include the minus sign in the boundary condition at $x = \ell$, following the convention of taking derivatives away from a node into an edge. The solution of Eq. (2.9) is $f(x) = Ae^{ikx} + Be^{-ikx}$. The boundary condition f'(0) = 0 implies that A = B. Because $-f'(\ell) = 0$, we obtain $k_m = \pi m/\ell$ with $m \in \{0, 1, 2, ...\}$. In quantum mechanics, m is known as a "quantum number". In this example, the quantum number m labels the vibrational modes of a particle in a box. We discard the trivial solution $f(x) \equiv 0$. The eigenfunctions that are associated with the eigenvalues k_m are

$$(2.10) f(x;m) = 2A\cos(\pi mx/\ell).$$

Adding a node between the two existing nodes in the interval $[0, \ell]$ does not change the solution (2.10). A degree-2 node with the Kirchhoff flux condition is thus equivalent to an uninterrupted edge [20, 111].

One can interpret the function $f(x;m) = 2A\cos(\pi mx/\ell)$ as a quantum wave function [see Figure 2(a)]. This requires us to normalize it such that

(2.11)
$$\int_0^\ell |f(x;m)|^2 dx = 1,$$

⁴Henceforth, when we use the term "Schrödinger equation", we always mean the linear, time-independent Schrödinger equation (*i.e.*, the Helmholtz equation).

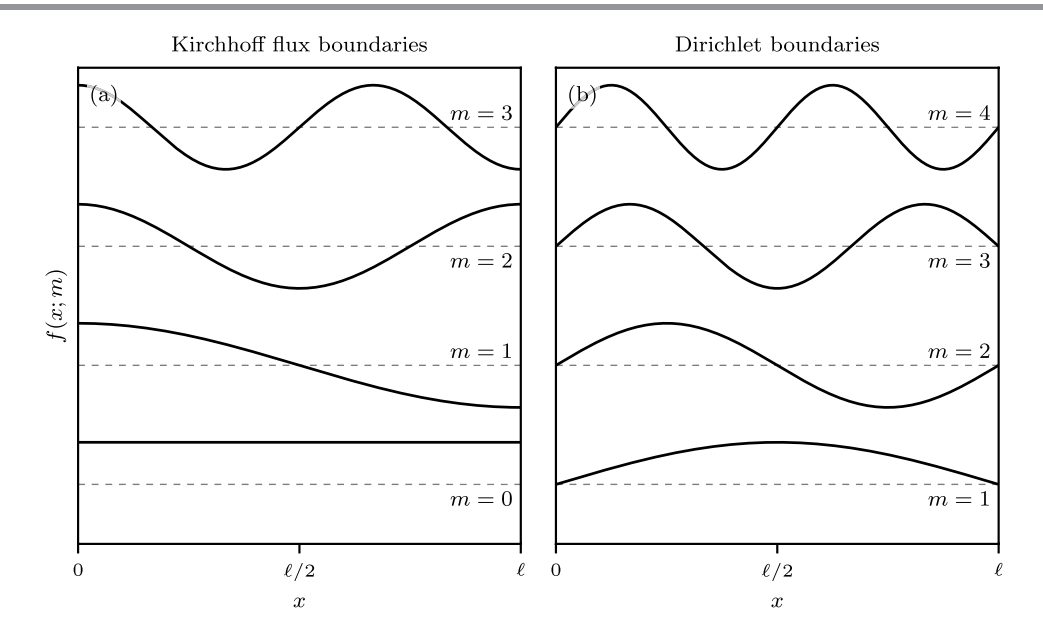


Figure 2. The eigenfunctions associated with Eq. (2.4) on a 2-node metric network with a single length- ℓ edge. The eigenfunctions are (a) $f(x;m) = \sqrt{2/\ell}\cos(k_m x)$ for Kirchhoff flux boundary conditions and (b) $f(x;m) = \sqrt{2/\ell}\sin(k_m x)$ for Dirichlet boundary conditions, where $k_m = \pi m/\ell$ is the wavenumber for $m \in \{0,1,2,\ldots\}$. We do not show the trivial solution $f(x;m=0) \equiv 0$ in panel (b).

which yields $A = 1/\sqrt{2\ell}$ and

(2.12)
$$f(x;m) = \sqrt{\frac{2}{\ell}}\cos(\pi mx/\ell).$$

As an alternative to the Kirchhoff flux condition (2.7), one can employ the Dirichlet condition (2.8). A calculation that is similar to the one above yields

(2.13)
$$f(x;m) = \sqrt{\frac{2}{\ell}}\sin(\pi mx/\ell).$$

Equation (2.13) describes a quantum particle in an infinite square well [see Figure 2(b)]. The case m = 0 is associated with the trivial solution $f(x; m = 0) \equiv 0$.

Consistent with the self-adjointness of the negative second-derivative operator with either Kirchhoff flux conditions or Dirichlet conditions (see Section 2.3), both Eqs. (2.12) and (2.13) give orthonormal bases with respect to the inner product $\langle f_{(u,v)}, g_{(u,v)} \rangle_{L^2((u,v))}$ (see Section 2.1). That is,

(2.14)
$$\int_0^{\ell} f(x; m) f(x; m') \, \mathrm{d}x = \delta_{mm'},$$

where the Kronecker delta function $\delta_{mm'}$ is 1 for m=m' and is 0 otherwise.

Although one can analytically solve the linear, time-independent Schrödinger equation on this 2-node network, it typically is necessary to use numerical methods to solve it on larger networks with Kirchhoff boundaries. When all of the edges of a metric network satisfy Dirichlet boundary conditions, one can simply use Eq. (2.13), as the edges all decouple from each other.

- 3. Numerical and analytical methods. There are multiple approaches to solve PDEs on metric networks. It is sometimes possible to obtain analytical solutions for small networks and PDEs that are analytically tractable on each edge. For larger networks and/or analytically intractable PDEs, it is necessary to employ numerical methods to obtain solutions. In Sections 3.1 and 3.2, we discuss two numerical approaches: a spectral method [42, 78] and a finite-difference method. Using a spectral method to numerically solve a PDE on a metric network with a self-adjoint operator (e.g., the 2-node system in Section 2.2) seems especially suitable, given the availability of a Fourier-like basis. Our spectral approach extends the spectral method in [42, 78] to account for degenerate eigenmodes. In Section 4, we present an illustrative example that demonstrates how degeneracies can arise in symmetric networks. In Appendix A, we relate the discussion of degeneracies to symmetry groups and their irreducible representations. Other numerical methods to study PDEs on metric networks include a discontinuous Galerkin method [42] and a finite-element method [8]. In Section 3.3, we discuss Weyl's law [7, 20] as a way to help track wavenumbers and their multiplicities when employing a spectral approach. Weyl's law for the Laplacian operator allows us to analytically estimate the number of eigenmodes up to a specified cutoff wavenumber when we employ a spectral approach to numerically solve PDEs on metric networks.
- **3.1.** A spectral method. One can express the solution of a linear PDE on a metric network in terms of an expansion (a so-called "spectral expansion") with respect to an appropriate orthonormal basis. One can construct such a basis using the eigenmodes of the self-adjoint operator $-\tilde{\Delta}$, which includes continuity conditions and boundary conditions at all nodes.

To compute the eigenmodes and their corresponding wavenumbers, we solve an eigenvalue problem that accompanies the Schrödinger equation

$$\tilde{\Delta}f = -k^2 f \,.$$

The function

(3.2)
$$f := (f_1(x_1), f_2(x_2), \dots, f_M(x_M))^{\top}$$

includes all functions $f_i(x_i)$ that are defined on associated edges, which have domains $[0, \ell_i]$. To make our notation more concise, we write $f_i(x_i)$ (with $i \in \{1, ..., M\}$) instead of $f_{(u,v)}(x_{(u,v)})$ (with $(u,v) \in \mathcal{E}$) and write ℓ_i instead of $\ell_{(u,v)}$. Some researchers (see, e.g., [42, 108]) use the same argument x for different edges, but we employ the notation x_i (with $i \in \{1, ..., M\}$) to account for the possibility that different edges can have distinct domains.

Solving Eq. (3.1) yields

$$f_i(x_i) = A_i \sin(kx_i) + B_i \cos(kx_i),$$

where one determines the coefficients A_i and B_i using the imposed continuity conditions and boundary conditions (i.e., the coupling conditions). A node u with degree $\deg(u)$ inherits $\deg(u) - 1$ equations from the continuity condition and 1 equation from the boundary condition. The total number of equations is thus $\sum_{u \in \mathcal{V}} \deg(u) = 2M$. These equations yield the homogeneous system

$$(3.4) T(k)X = 0$$

for the coefficient vector $X = (A_1, B_1, ..., A_M, B_M)^{\top} \in \mathbb{R}^{2M}$. The nontrivial solutions of Eq. (3.4) require the coupling-condition matrix T(k) to be singular (i.e., $\det(T(k)) = 0$). We refer to the corresponding values k_m (with quantum number $m \in \{1, 2, ...\}$) as the "characteristic wavenumbers" in a metric network.⁵

For each characteristic wavenumber k_m , we determine the null space of $T(k_m)$. If its dimension $\dim(\ker T(k_m))$ is larger than 1, there exist degenerate eigenmodes. Let $A_1^{mn}, B_1^{mn}, \ldots, A_M^{mn}, B_M^{mn}$ (with $n \in \{1, \ldots, \dim(\ker T(k_m))\}$) denote the coefficients of the (potentially degenerate) eigenmodes. The eigenmodes that are associated with k_m are

(3.5)
$$f^{mn} = \begin{pmatrix} A_1^{mn} \sin(k_m x_1) + B_1^{mn} \cos(k_m x_1) \\ A_2^{mn} \sin(k_m x_2) + B_2^{mn} \cos(k_m x_2) \\ \vdots \\ A_M^{mn} \sin(k_m x_M) + B_M^{mn} \cos(k_m x_M) \end{pmatrix}.$$

One can normalize the eigenmodes f^{mn} using the inner product

(3.6)
$$\langle f^{mn}, f^{mn} \rangle_{L^2(\mathcal{G})} = \sum_{i=1}^M \int_0^{\ell_i} f_i^{mn}(x) f_i^{mn}(x) \, \mathrm{d}x \,.$$

Given a set $\{f^{mn}\}$ of orthonormal eigenmodes, we can construct a spectral expansion for another function that is defined on the same metric network. It has been shown [42] that the spectral-expansion coefficients decay faster than any polynomial (a property that is known as "spectral convergence") for any function in $L^2(\mathcal{G})$ with compact support on all edges for which the function is nonzero. For functions in $L^2(\mathcal{G})$ that do not have compact support on all such edges, the expansion coefficients decay with the quantum number m as m^{-4} .

In our numerical calculations, we use the described spectral approach to construct the solutions of PDEs on metric networks by expanding these solutions in the eigenmodes $\{f^{mn}\}$. We give further details in Section 5.1, where we consider the Poisson equation on several metric networks.

3.2. Finite differences. Another way to numerically solve a PDE on a metric network is to use a finite-difference approximation. In the systems that we study in the present paper, we need to discretize both first derivatives (because of Kirchhoff boundary conditions) and second derivatives (e.g., for Schrödinger operators). We denote the step size in a discretized edge domain $[0, \ell_i]$ by $h_i := \ell_i/N_i$ (with $i \in \{1, ..., M\}$), where N_i is the number of intervals that we use to discretize $[0, \ell_i]$. In Figure 3, we show a schematic illustration of our discretization scheme.

One possible discretization of the second derivative of $f_i(x_i)$ is

(3.7)
$$f_i''(x_i) := \frac{\mathrm{d}^2}{\mathrm{d}x^2} f_i(x_i) = \frac{f_i(x_i + h_i) - 2f_i(x_i) + f_i(x_i - h_i)}{h_i^2} + \mathcal{O}(h_i^2).$$

One can also employ higher-order discretizations or use implicit methods. We write $f_{i,j}$ as a shorthand notation for $f_i(jh_i)$ (with $j \in \{0, ..., N_i\}$).

⁵We prefer the term "characteristic wavenumber" to "resonant frequency" [42, 108] because the quantity k is physically a wavenumber, rather than a frequency.

Figure 3. A finite-difference discretization of an edge i with length ℓ_i . We employ a uniform discretization with step size $h_i = \ell_i/N_i$.

Consider a Schrödinger equation of the form (2.9) on each of the M edges of a metric network. We summarize the discretized second derivatives (3.7) in a square matrix. Most of the matrix entries are 0, so we use a sparse-matrix representation when implementing our numerical solvers.

For Dirichlet boundary conditions, $f_i(0) = f_{i,0} = 0$ and $f_i(\ell_i) = f_{i,N_i} = 0$ for all edges i. Therefore, the second derivatives at $x_i = h_i$ and $x_i = \ell_i - h_i$ are $f''_{i,1} = (f_{i,2} - 2f_{i,1})/h_i^2 + \mathcal{O}(h_i^2)$ and $f''_{i,N_i-1} = (f_{i,N_i-2} - 2f_{i,N_i-1})/h_i^2 + \mathcal{O}(h_i^2)$, respectively. For one edge with Dirichlet boundaries, the discretized version of the generalized Laplacian $\tilde{\Delta}$ [see Eq. (3.1)] is thus

(3.8)
$$\tilde{\Delta}_{h_i} = \frac{1}{h_i^2} \begin{pmatrix} -2 & 1 & 0 & \cdots & 0 & 0\\ 1 & -2 & 1 & \cdots & 0 & 0\\ 0 & 1 & -2 & \cdots & 0 & 0\\ \vdots & \vdots & \vdots & \ddots & \vdots & \vdots\\ 0 & 0 & 0 & \cdots & 1 & -2 \end{pmatrix} \in \mathbb{R}^{(N_i - 1) \times (N_i - 1)}.$$

Solving the discrete Schrödinger equation (3.1) using the discrete Laplace–Dirichlet operator (3.8) yields

(3.9)
$$f_{i,j'} \propto \sin\left(\frac{\pi m j'}{N_i}\right), \quad j' \in \{1, \dots, N_i - 1\},$$

which is a discrete analogue of the sine eigenfunction (2.13). The corresponding eigenvalues $k_{i,m}$ satisfy

$$(3.10) -k_{i,m}^2 = -\frac{4}{h_i^2} \sin\left(\frac{\pi m}{2N_i}\right)^2 = -\frac{m^2 \pi^2}{\ell_i^2} + \mathcal{O}(m^4 h_i^2), \quad m \in \{1, \dots, N_i - 1\}.$$

These eigenvalues yield the eigenvalues for the continuous system (2.9) in the limit $h_i \to 0$ [42, 49].

For a single edge with Kirchhoff (i.e., Neumann) boundaries, $f'_{i,0} = (f_{i,1} - f_{i,-1})/(2h_i) + \mathcal{O}(h_i^2) = 0$ and $f'_{i,N_i} = (f_{i,N_i-1} - f_{i,N_i+1})/(2h_i) + \mathcal{O}(h_i^2) = 0$. We thus obtain $f_{i,1} = f_{i,-1} + \mathcal{O}(h_i^3)$ and $f_{i,N_i-1} = f_{i,N_i+1} + \mathcal{O}(h_i^3)$, so the second derivatives at the boundaries are $f''_{i,0} = 2(f_{i,1} - f_{i,0})/h_i^2 + \mathcal{O}(h_i)$ and $f''_{i,N_i} = 2(f_{i,N_i-1} - f_{i,N_i})/h_i^2 + \mathcal{O}(h_i)$. We have introduced "ghost" points at $x_i = -h_i$ and $x_i = \ell_i + h_i$ to write second-order finite-difference approximations of $f'_{i,0}$ and f'_{i,N_i} . The lowest-order approximation determines the overall order of the employed approximation scheme. The discretized version of the generalized Laplacian $\tilde{\Delta}$ for a single Kirchhoff edge is

⁶One can use higher-order finite-difference approximations at boundary points to maintain the same approximation order throughout each edge, including at the boundaries. Additionally, to ensure consistency throughout a system's domain, one uses the same approximation order for all edges.

(3.11)
$$\tilde{\Delta}_{h_i} = \frac{1}{h_i^2} \begin{pmatrix} -2 & 2 & 0 & \cdots & 0 & 0 \\ 1 & -2 & 1 & \cdots & 0 & 0 \\ 0 & 1 & -2 & \cdots & 0 & 0 \\ \vdots & \vdots & \vdots & \ddots & \vdots & \vdots \\ 0 & 0 & 0 & \cdots & 2 & -2 \end{pmatrix} \in \mathbb{R}^{(N_i+1)\times(N_i+1)}.$$

Solving the discrete Schrödinger equation (3.1) using the discrete Laplace–Kirchhoff operator (3.11) yields

(3.12)
$$f_{i,j'} \propto \cos\left(\frac{\pi m j'}{N_i}\right), \quad j' \in \{0, \dots, N_i\},$$

which is a discrete analogue of the cosine eigenfunction (2.12). The corresponding eigenvalues $k_{i,m}$ (with $m \in \{0, ..., N_i\}$) satisfy (3.10). In signal processing and data compression, the matrices (3.8) and (3.11) are known as the discrete sine transform and discrete cosine transform, respectively [165].

It is straightforward to simulate the Schrödinger equation (2.9) on a metric network with Dirichlet boundaries. One just needs to construct a block-diagonal matrix in which each block represents the Laplace-Dirichlet operator (3.8) that is associated with a specified edge. Recall that Dirichlet boundaries imply that edges are isolated, resulting in noninteracting "signals". The situation is different for metric networks with Kirchhoff flux boundaries. To construct the discretized generalized Laplacian for a metric network with Kirchhoff boundaries, one possible starting point is to use a block-diagonal matrix in which each block represents the Laplace-Kirchhoff operator (3.11) that is associated with a specified edge. One then needs to adjust the matrix entries such that edges interact through Kirchhoff flux conditions at the associated nodes. Consider a node u at which the edges $i \in \mathcal{E}_u$ terminate or originate. Let f_0 denote the value of f at node u. Regardless of the edge's orientation, let $f_{i,1}$ denote the value of the function f_i at the discretization point next to node u. As in [42], we use a central second-order scheme to approximate the first derivative at node u and thereby obtain

(3.13)
$$2\frac{\sum_{i \in \mathcal{E}_u} \frac{f_{i,1} - f_0}{h_i}}{\sum_{i \in \mathcal{E}} h_i} = -k^2 f_0.$$

We derive (3.13) by applying the Kirchhoff flux condition at the boundary node u (where the function takes the value f_0) and at a ghost point that is adjacent to that node. We then eliminate the ghost point using the centered finite-difference approximation (3.7) to obtain (3.13). For each node with Kirchhoff boundaries, one needs to incorporate the associated expression from the left-hand side of Eq. (3.13) into the discrete generalized Laplacian (3.11).

Equation (3.13) gives one way to couple the dynamics that are associated with different edges. In a recent paper [14], Avdonin et al. proposed a variational method as an alternative approach to establish coupling conditions in a discrete linear wave equation on a metric network.

Although finite differences provide a relatively straightforward way to numerically solve the Schrödinger equation (3.1) on a metric network, a downside of this approach is the $\mathcal{O}(m^4h_i^2)$ error term in $k_{i,m}^2$ [see Eq. (3.10)] for both Dirichlet and Kirchhoff boundary conditions.

In Figure 4, we show the absolute error in the difference between the numerical values of $k_{i,m}^2$ and their corresponding analytical values as a function of m. We consider two metric networks: a 2-node network with a single edge and Dirichlet boundaries [see Figure 4(a)] and a star network with N=4 nodes, M=3 edges, and Kirchhoff flux boundaries [see Figure 4(b)]. The observed error scaling is consistent with the aforementioned quartic dependence on m.

We show a schematic illustration of a 3-edge star network in Figure 5. We will revisit this example in Section 4 and in Appendix A. In the present discussion, our objective is to emphasize that employing finite differences may not be practical when attempting to capture signals with large wavenumers (*i.e.*, small wavelengths). However, a finite-difference approach can be useful in situations with small wavenumbers. It can also provide benchmark results to use as a baseline when employing other numerical techniques, such as the spectral method in Section 3.1.

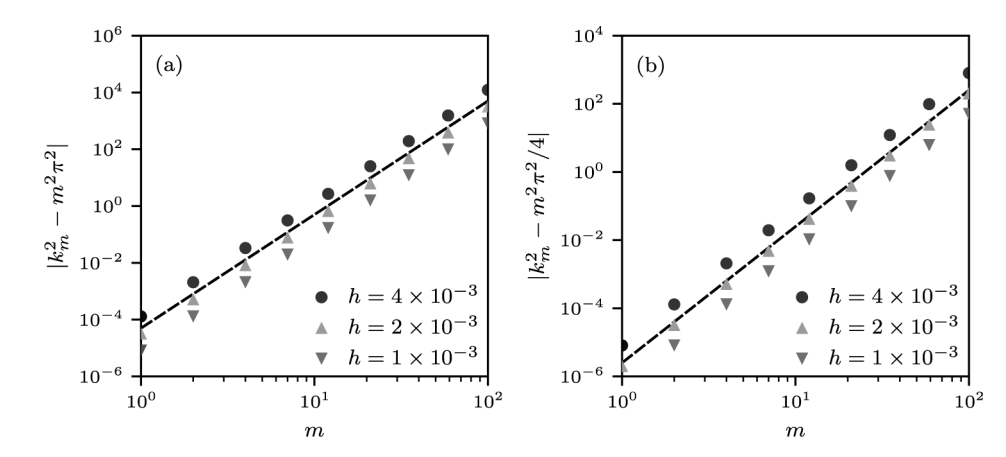


Figure 4. Error scaling of our finite-difference method for the Schrödinger equation (3.1) on metric networks. We show the absolute error of the difference between the numerical values of k_m^2 (where k_m is the mth eigenvalue) and the corresponding analytical values of k_m^2 as a function of the quantum number m. Different types of markers correspond to different step sizes h. (a) The error scaling for a metric network with 2 nodes, a single length-1 edge, and Dirichlet boundaries. (b) The error scaling for a star network with 4 nodes, 3 length-1 edges, and Kirchhoff flux boundaries. In both examples, the observed error scaling is consistent with a quartic dependence on m, as indicated by the dashed black line [see Eq. (3.10)].

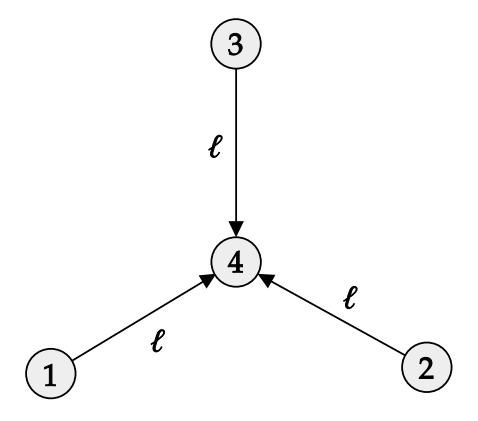


Figure 5. A metric star network with N=4 nodes and M=3 edges. The length of each edge is ℓ .

3.3. Weyl's law. It can be challenging to identify all of the characteristic wavenumbers in an interval due to the rounding errors that occur when numerically determining if T(k) [see Eq. (3.4)] becomes singular and when working with discrete Laplacian operators (see Section 3.2). Therefore, it is useful to estimate the number of characteristic wavenumbers up to a specified cutoff value.

Let $N_{\mathcal{G}}(k)$ denote the characteristic-wavenumber counting function, which counts the number of characteristic wavenumbers k' that satisfy $k'^2 \leq k^2$. That is,

(3.14)
$$N_{\mathcal{G}}(k) := \{ |k': k'^2 \le k^2 \text{ and } \det(T(k')) = 0 | \}.$$

According to Weyl's law [20, 22],

$$(3.15) N_{\mathcal{G}}(k) = \frac{\mathcal{L}}{\pi}k + \mathcal{O}(1),$$

where $\mathcal{L} = \sum_{i=1}^{M} \ell_i$ is the total length of the edges. Additionally, the counting function $N_{\mathcal{G}}(k)$ satisfies

(3.16)
$$\frac{\mathcal{L}}{\pi}k - M \le N_{\mathcal{G}}(k) \le \frac{\mathcal{L}}{\pi}k + N.$$

There is also an analogue of Weyl's law for resonances on networks [105].⁷ In that context, deviations in the counting function $N_{\mathcal{G}}(k)$ from Weyl's law have been studied both theoretically [58, 59] and experimentally [118].

4. Illustrative example: A star network. Consider the Schrödinger equation (3.1) on a metric star network \mathcal{G} with N=4 nodes, M=3 equal-length edges, and Kirchhoff flux conditions at each node. We seek to compute the characteristic wavenumbers and their corresponding eigenmodes. This example is analytically tractable, but we also use a numerical spectral approach that we will continue to use subsequently. Our comparison of analytical and numerical results for this star network enables us to examine the numerical-resolution requirements of the spectral approach in Section 3.1.

Let $T_{\lambda}(k)$ (with a 3-pointed star as a subscript) denote the coupling-condition matrix [see Eq. (3.4)] that is associated with the 3-edge star network with Kirchhoff flux conditions. Specifically,

$$(4.1) T_{\blacktriangle}(k) = \begin{pmatrix} 1 & 0 & 0 & 0 & 0 & 0 \\ 0 & 0 & 1 & 0 & 0 & 0 \\ 0 & 0 & 0 & 0 & 1 & 0 \\ \sin(k\ell) & \cos(k\ell) & -\sin(k\ell) & -\cos(k\ell) & 0 & 0 \\ \sin(k\ell) & \cos(k\ell) & 0 & 0 & -\sin(k\ell) & -\cos(k\ell) \\ -\cos(k\ell) & \sin(k\ell) & -\cos(k\ell) & \sin(k\ell) & -\cos(k\ell) & \sin(k\ell) \end{pmatrix}.$$

⁷For more information about such resonances, see [105, 118] and references therein.

⁸One can obtain analytical insights even for 3-edge metric star networks with unequal edge lengths. Barra and Gaspard [18] derived an analytical description of the distribution of level spacings (*i.e.*, the differences between consecutive energy levels) for the Schrödinger operator [see Eq. (3.1)] on such metric networks.

Alternatively, we can first establish that $A_1 = A_2 = A_3 = 0$ because nodes 1, 2, and 3 are degree-1 nodes with the Kirchhoff flux condition (see Section 2.4). Therefore, the eigenmodes are cosine functions. The remaining Kirchhoff and continuity conditions at node 4 yield

(4.2)
$$\widetilde{T}_{\mathbf{A}}(k) = \begin{pmatrix} \cos(k\ell) & -\cos(k\ell) & 0\\ \cos(k\ell) & 0 & -\cos(k\ell)\\ \sin(k\ell) & \sin(k\ell) & \sin(k\ell) \end{pmatrix}.$$

The nontrivial solution of Eq. (3.4) satisfies $\det(\widetilde{T}_{\star}(k)) = 0$. This yields

$$(4.3) 3\cos(k\ell)^2\sin(k\ell) = 0.$$

There is a constant mode $(1,1,1)^{\top}/\sqrt{3\ell}$ with characteristic wavenumber 0. The other characteristic wavenumbers are $k_m = \pi m/(2\ell)$ (with $m \in \{1,2,\ldots\}$). The algebraic multiplicity of k_m is

(4.4)
$$\mu_{T(k_m)} = \begin{cases} 2, & m \text{ is odd} \\ 1, & m \text{ is even.} \end{cases}$$

For odd m, there are two degenerate eigenmodes:

(4.5)
$$f^{m1} = \frac{1}{\sqrt{\ell}} \begin{pmatrix} \cos(k_m x) \\ 0 \\ -\cos(k_m x) \end{pmatrix} \quad \text{and} \quad f^{m2} = \frac{1}{\sqrt{\ell}} \begin{pmatrix} \cos(k_m x) \\ -\cos(k_m x) \\ 0 \end{pmatrix}.$$

This geometric multiplicity (i.e., the dimension of the eigenspace that is spanned by the two degenerate eigenmodes f^{m1} and f^{m2}) equals the dimension of one of the irreducible representations of the underlying symmetry group, which is the permutation group S_3 (see Appendix A). For even m, the eigenmode is

(4.6)
$$f^{m1} = \sqrt{\frac{2}{3\ell}} \begin{pmatrix} \cos(k_m x) \\ \cos(k_m x) \\ \cos(k_m x) \end{pmatrix}.$$

Observe that $\langle f^{m1}, f^{m2} \rangle_{L^2(\mathcal{G})} = 1/2$ if m is odd and that $\langle f^{m1}, f^{m'1} \rangle_{L^2(\mathcal{G})} = \delta_{mm'}$ if m is even. In Figure 6, we show the eigenmodes for the 3-edge metric star network for $m \in \{1, 2, 3, 4\}$. The solid blue curves show the analytically obtained eigenmodes from Eqs. (4.5) and (4.6). We also examine the ability of our spectral numerical approach to identify the characteristic wavenumbers and their corresponding eigenmodes with sufficient numerical precision. For each characteristic wavenumber k_m , the coupling-condition matrix $T(k_m)$ is singular (i.e., $\det(T(k_m)) = 0$). However, the determinant is not an appropriate indicator of singularity in numerical calculations. Following [42, 78], we use the condition number $\kappa(T(k))$ to determine whether or not a certain value of k is a characteristic wavenumber k_m . For values of k that

⁹In our finite-difference approach, we initially treat all edges of a metric network separately and use the two indices in $k_{i,m}$ to label the characteristic wavenumber m that is associated with edge i [see Eq. (3.10)]. After applying the coupling conditions, all edges have the same characteristic wavenumber k_m . Therefore, in the present example, we need only the index m for the characteristic wavenumbers.

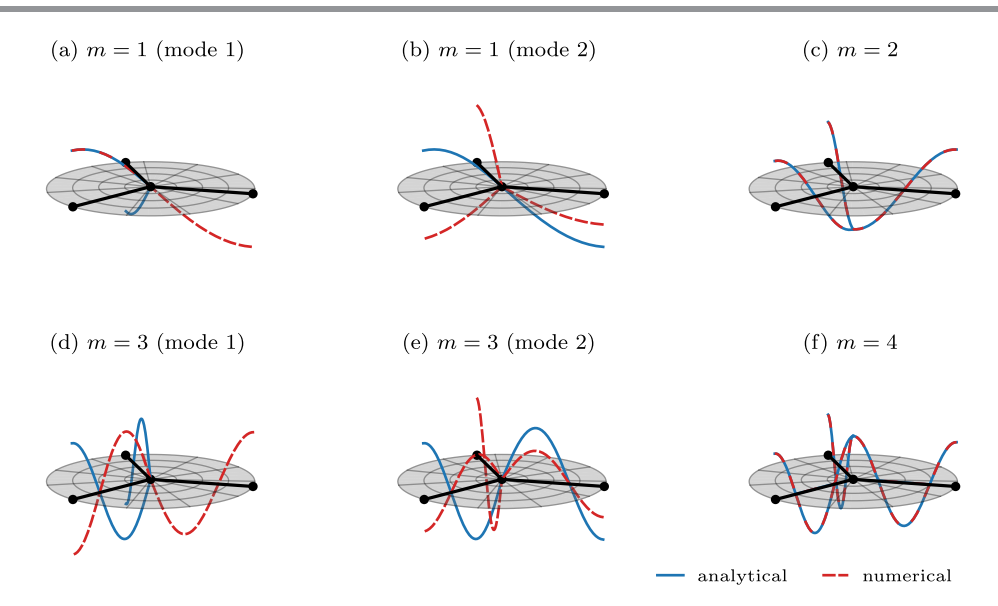


Figure 6. Eigenmodes of the Schrödinger equation (3.1) on a metric star network with N=4 nodes (black disks) and M=3 edges (black lines). All edges have length ℓ and Kirchhoff boundaries. For $m\in\{1,3\}$, the eigenmodes are degenerate [see Eq. (4.5)]; they are not degenerate for $m\in\{2,4\}$ [see Eq. (4.6)]. The solid blue curves show the analytical solutions f^{m1} and f^{m2} for odd m [see Eq. (4.5)] and f^{m1} for even m [see Eq. (4.6)]. We also determine the characteristic wavenumbers k_m numerically by searching for minima of the inverse condition number $\kappa(T(k))^{-1}$ of the coupling-condition matrix $T_{\mathbf{k}}(k)$ [see Eq. (4.1)]. We then use these numerically obtained k_m to compute the null space (and hence the eigenmodes) of the coupling-condition matrix using a QR decomposition. We indicate the associated numerical eigenmodes with dashed red curves. The numerical eigenmode in panels (a,d) is $(\cos(k_m x), -\cos(k_m x), 0)^{\top}/\sqrt{\ell}$, which equals f^{m2} in Eq. (4.5). The numerical eigenmode in panels (b,e) is $(-\cos(k_m x), -\cos(k_m x), 2\cos(k_m x))^{\top}/\sqrt{3\ell}$, which equals $-(2/\sqrt{3})f^{m1}+(1/\sqrt{3})f^{m2}$. Unlike f^{m1} and f^{m2} , the two numerical eigenmodes are orthonormal [see Eqs. (4.9) and (4.10)]. See https://metricnets.streamlit.app/ for a web application to listen to Schrödinger eigenmodes in the depicted network.

are close to k_m , the coupling-condition matrix is almost singular, so the condition number $\kappa(T(k))$ increases significantly as $k \to k_m$. We compute $\kappa(T(k))$ using the formula

(4.7)
$$\kappa(T(k)) = \frac{\sigma_{\max}(T(k))}{\sigma_{\min}(T(k))},$$

where $\sigma_{\max}(T(k))$ and $\sigma_{\min}(T(k))$ are the maximum and minimum singular values, respectively. There exist sparse singular-value-decomposition (SVD) methods in many numerical software packages (e.g., SciPy) that allow one to compute the singular values of large, sparse matrices.

To numerically determine characteristic wavenumbers, we initially compute the inverse condition numbers $\kappa(T(k))^{-1}$ for a range of values of k [see Figure 7(a)]. For the star network, we consider $k \in [0, 10^2]$ and choose 2×10^3 evenly spaced values of k. We consider a value of k to be a candidate for a characteristic wavenumber if $\kappa(T(k))^{-1} < 10^{-2}$. We then minimize $\kappa(T(k))^{-1}$ using the candidate characteristic wavenumbers as initial values $k^{(0)}$. To minimize the scalar function $\kappa(T(k))^{-1}$, we employ a constrained Brent method [41]. (It is implemented in the minimize_scalar function in SciPy.) For an initial value $k^{(0)}$, we set the interval bound of k to $[k^{(0)} - 0.1, k^{(0)} + 0.1]$. We use machine precision as an acceptable absolute error for the

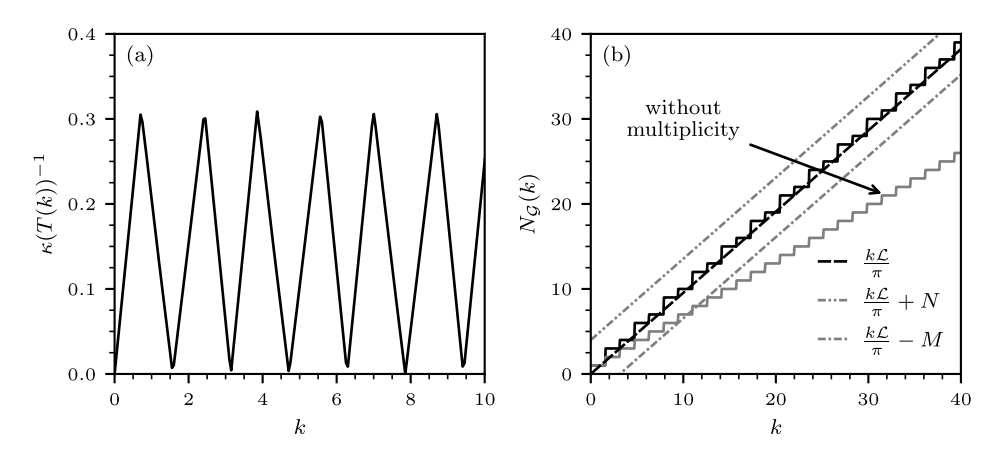


Figure 7. The inverse condition number $\kappa(T(k))^{-1}$ and characteristic-wavenumber counting function $N_{\mathcal{G}}(k)$ for a 3-edge metric star network. The length of each edge is $\ell=1$. (a) We plot the inverse condition number $\kappa(T(k))^{-1}$ as a function of the characteristic wavenumber k. Observe that $\kappa(T(k))^{-1}$ is small near the characteristic wavenumbers $k_m = \pi m/2$ (with $m \in \{1, 2, ...\}$). (b) We plot the characteristic-wavenumber counting function $N_{\mathcal{G}}(k)$ (solid black curve) as a function of k and show Weyl's law $N_{\mathcal{G}}(k) = k\mathcal{L}/\pi$ (dashed black curve), where $\mathcal{L} = 3\ell = 3$. In this plot, we include the "zero mode" (for which $k_{m=0} = 0$) in $N_{\mathcal{G}}(k)$. The dash-dotted and dash-dot-dotted gray lines, respectively, indicate the lower and upper bounds of Weyl's law [see Eq. (3.16)]. The algebraic multiplicity of k_m is 2 for odd m and 1 for even m. We thus have to count k_m twice for odd m. In our numerical computations, we do this by counting k_m using its corresponding null-space dimension dim(ker $T(k_m)$). The solid gray curve shows the characteristic-wavenumber counting function without accounting for the degeneracy for odd m.

convergence of k. The best choices for the range and number of values of k, the optimization bounds, and the convergence criterion depend on the specific system that one is studying. After performing minimizations for all candidate characteristic wavenumbers, we obtain a set of values of k_m for which $\kappa(T(k_m))^{-1}$ is close to 0. We then round the values of k_m to the nearest number with a specified number of digits and obtain a set of distinct numerical characteristic wavenumbers.

Armed with a set of characteristic wavenumbers k_m , we seek to compute the vectors that span the null space of $T(k_m)$. To do this, one can use a method that is based on an SVD or a QR decomposition. Because degenerate eigenmodes can occur in PDEs on metric networks [see Eq. (3.5)], it is possible that the null space of $T(k_m)$ is spanned by multiple eigenvectors, rather than by a single eigenvector. When employing an SVD, one has to identify the singular vectors that are associated with near-0 singular values within some tolerance. To obtain the null space using a QR decomposition of a matrix, we first perform the QR decomposition on the transpose of the matrix. We then identify the columns of the orthonormal matrix Q that are associated with the rows of the upper triangular matrix R whose diagonal entries are approximately 0 within a specified tolerance. In Algorithm 4.1, we summarize our numerical method to determine wavenumbers and eigenmodes.

¹⁰The sparse-matrix SVD in some versions of SciPy can produce erroneous null-space vectors (see, e.g., https://github.com/scipy/scipy/issues/11406). Therefore, we use a sparse-matrix QR decomposition method (which is available at https://github.com/yig/PySPQR) that implements a Python wrapper for the SUITESPARSEQR function in the sparse QR implementation of MATLAB.

Algorithm 4.1. Compute the characteristic wavenumbers and their corresponding eigenmodes.

```
1: Inputs:
```

k_arr, Δk , cutoff, precision, T(), INV_COND_NUM(), MINIMIZE(), NULLSPACE()

2: Outputs:

k_m_arr, f_m_arr

3: Initialize:

char_wavenum_cand, k_m_arr, f_m_arr

- 4: for k in k_arr do
- 5: $kappa_inv \leftarrow INV_COND_NUM(k,T)$
- 6: **if** kappa_inv < cutoff **then** \triangleright Check that the inverse condition number is sufficiently small to be a candidate characteristic wavenumber
- 7: $\operatorname{char}_{\operatorname{a}}\operatorname{wavenum}_{\operatorname{cand.append}}(k)$
- 8: end if
- 9: end for
- 10: for $k^{(0)}$ in char_wavenum_cand do
- 11: $k_m \leftarrow \text{MINIMIZE}(\text{INV_COND_NUM}, \text{args} = (T), \text{bounds} = (k^{(0)} \Delta k, k^{(0)} + \Delta k))$
- 12: $k_m_arr \leftarrow k_m$
- 13: end for
- 14: rounded_elements \leftarrow [ROUND(k_m , precision) for k_m in k_m_arr]
- 16: for k in k_m_arr do
- 17: $V \leftarrow \text{NULLSPACE}(k,T)$
- 18: $f_m_{arr.append}(V)$
- 19: end for
- 20: **return** k_m_arr, f_m_arr

For our 3-edge star network, we show the numerically obtained eigenmodes as dashed red curves in Figure 6. These numerical eigenmodes coincide with the analytical eigenmodes for $m \in \{2,4\}$. However, our numerical eigenmodes do not coincide with our choice of analytical eigenmodes for $m \in \{1,3\}$. The numerical eigenmodes in Figures 6(a,d) are $(\cos(k_m x), -\cos(k_m x), 0)^{\top}/\sqrt{\ell}$, which equals f^{m2} in Eq. (4.5). In Figures 6(b,e), the numerical eigenmode is

(4.8)
$$\frac{1}{\sqrt{3\ell}} \begin{pmatrix} -\cos(k_m x) \\ -\cos(k_m x) \\ 2\cos(k_m x) \end{pmatrix},$$

which equals $-(2/\sqrt{3})f^{m1} + (1/\sqrt{3})f^{m2}$. The numerically obtained degenerate eigenmodes lie in span $\{f^{m1}, f^{m2}\}$. Unlike the analytical eigenmodes f^{m1} and f^{m2} , the two numerical eigenmodes are orthonormal. That is,

$$\left\langle -\frac{2}{\sqrt{3}}f^{m1} + \frac{1}{\sqrt{3}}f^{m2}, f^{m2} \right\rangle_{L^{2}(\mathcal{G})} = -\frac{2}{\sqrt{3}} \left\langle f^{m1}, f^{m2} \right\rangle_{L^{2}(\mathcal{G})} + \frac{1}{\sqrt{3}} \left\langle f^{m2}, f^{m2} \right\rangle_{L^{2}(\mathcal{G})} = 0$$

and

$$\left\| -\frac{2}{\sqrt{3}} f^{m1} + \frac{1}{\sqrt{3}} f^{m2} \right\|_{L^{2}(\mathcal{G})}^{2} = -\frac{4}{3} \left\langle f^{m1}, f^{m2} \right\rangle_{L^{2}(\mathcal{G})} + \frac{4}{3} \left\| f^{m1} \right\|_{L^{2}(\mathcal{G})}^{2} + \frac{1}{3} \left\| f^{m2} \right\|_{L^{2}(\mathcal{G})}^{2} = 1.$$

If a set of degenerate eigenmodes is not already orthonormal, one can make them orthonormal by using the Gram-Schmidt algorithm.

To ensure that our numerical approach identifies all of the characteristic wavenumbers in an interval, we use Weyl's law (see Section 3.3) to compare the numerically obtained wavenumber-counting function $N_{\mathcal{G}}(k)$ to its estimate $k\mathcal{L}/\pi$. For the 3-edge star network with equal edge lengths $\ell=1$, the total edge length \mathcal{L} is 3. In Figure 7(b), we see that the numerically computed counting function $N_{\mathcal{G}}(k)$ (solid black curve) closely resembles the estimate from Weyl's law (dashed black curve). Recall that k_m has an algebraic multiplicity of 2 when m is odd and an algebraic multiplicity of 1 when m is even. Therefore, for odd m, we have to count k_m twice. In our numerical computations, we achieve this by using the null-space dimension $\dim(\ker T(k_m))$ to count k_m . If we do not consider the degeneracy for odd m (solid gray curve), the characteristic-wavenumber counting function does not match Weyl's law. Visible differences between numerically computed counting functions and estimates of counts from Weyl's law can highlight the need to refine a numerical method.

5. Numerical examples with various PDEs. We now study the Poisson equation, the heat equation, and the wave equation on metric networks. These PDEs, respectively, are fundamental types of elliptic, parabolic, and hyperbolic PDEs. They complement our examinations of the Schrödinger equation in Section 2.4 [see Eq. (2.9)] and Section 3 [see Eq. (3.1)]. We consider metric networks with up to about 10⁴ nodes and about 10⁴ edges. These networks are much larger than those in most studies of metric networks. (Most such studies typically examine networks with very few nodes and edges.) In our numerical computations, we find that the implemented spectral approach is valuable for identifying eigenmodes in a metric network. However, it has difficulty at accurately determining a large number of eigenmodes, especially when they are degenerate. This may hinder the ability of this approach to accurately resolve solutions of PDEs on metric networks.

5.1. Poisson equation. The Poisson equation

$$\tilde{\Delta}\phi = \rho$$

describes the potential field ϕ that is associated with a function ρ (e.g., a mass or electrical-charge distribution). The Poisson equation, which is an elliptic PDE, also describes the steady state of the heat equation with a heat source (see Section 5.2). As before, the operator $\tilde{\Delta}$ in Eq. (5.1) is the generalized Laplacian that includes continuity conditions and boundary conditions at all nodes. The Fredholm solvability condition forces ρ to be orthogonal to the kernel of the generalized Laplacian; this kernel is spanned by the constant function.

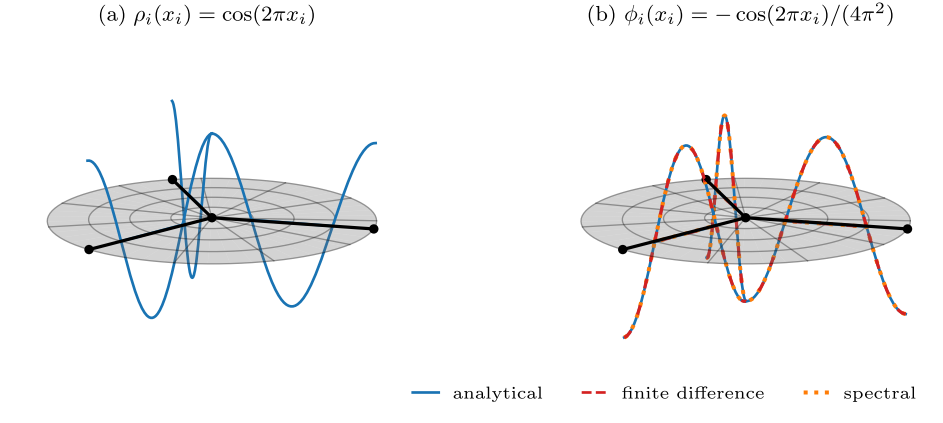


Figure 8. Solution of the Poisson equation (5.1) on a metric star network with N=4 nodes (black disks) and M=3 edges (black lines). All edges $i \in \{1,2,3\}$ have length $\ell_i=1$ and Kirchhoff boundaries. (a) The source term $\rho_i(x_i) = \cos(2\pi x_i)$ (solid blue curve) for each edge i. (b) The solution $\phi_i(x_i) = -\cos(2\pi x_i)/(4\pi^2)$ (solid blue curve) of the Poisson equation for each edge i. The dashed red and dotted orange curves indicate numerical solutions using finite-difference and spectral methods, respectively. These curves almost overlap the solid blue analytical solution and are practically indistinguishable at this scale.

Consider the 3-edge star network from Section 3 (see Figure 5) and set

for all edges $i \in \{1, 2, 3\}$ [see Figure 8(a)]. This choice of ρ satisfies the Fredholm solvability condition. Consequently, the solution ϕ is not unique. We impose uniqueness by requiring ϕ to be orthogonal to the kernel of the generalized Laplacian. We set the lengths ℓ_i of all edges to 1. All boundaries are of Kirchhoff type, so the solution of the corresponding Poisson equation (5.1) is $\phi_i(x_i) = -\cos(2\pi x_i)/(4\pi^2)$ [see Figure 8(b)].

Recall that the generalized negative Laplacian with Kirchhoff boundaries is self-adjoint and hence has an orthonormal eigenbasis (see Section 2.3). We employ a spectral approach and expand the solution of Eq. (5.1) using the eigenbasis of $-\tilde{\Delta}$. To do this, we use Algorithm 4.1 with the same parameters as in Section 4 to compute characteristic wavenumbers. We then construct the solution of the Poisson equation (5.1) using orthonormal spectral solutions f^{mn} (with $m \in \{1, 2, ...\}$ and $n \in \{1, ..., \dim(\ker T(k_m))\}$) that are associated with Eq. (3.1). That is,

(5.3)
$$\phi = \sum_{m,n} a_{mn} f^{mn} \text{ and } a_{mn} = -b_{mn}/k_m^2,$$

where $b_{mn} = \langle f^{mn}, \rho \rangle_{L^2(\mathcal{G})}^{11}$ Equation (5.3) is an exact spectral expansion. By summing over all $a_{mn}f^{mn}$, we obtain the exact solution ϕ . However, in practice, one has to truncate the sum at a certain value of m.

For our finite-difference solution of Eq. (5.1), we set the number of discretization intervals to $N_i = 1000$ for all edges $i \in \{1, 2, 3\}$. To discretize the generalized Laplacian $\tilde{\Delta}$, we use

¹¹Because the constant "zero mode" of the Schrödinger equation (3.1) with Kirchhoff boundaries has an associated eigenvalue of 0, the Fredholm alternative guarantees that $b_{01} = 0$ [42]. Therefore, the sum over m in Eq. (5.3) starts at m = 1.

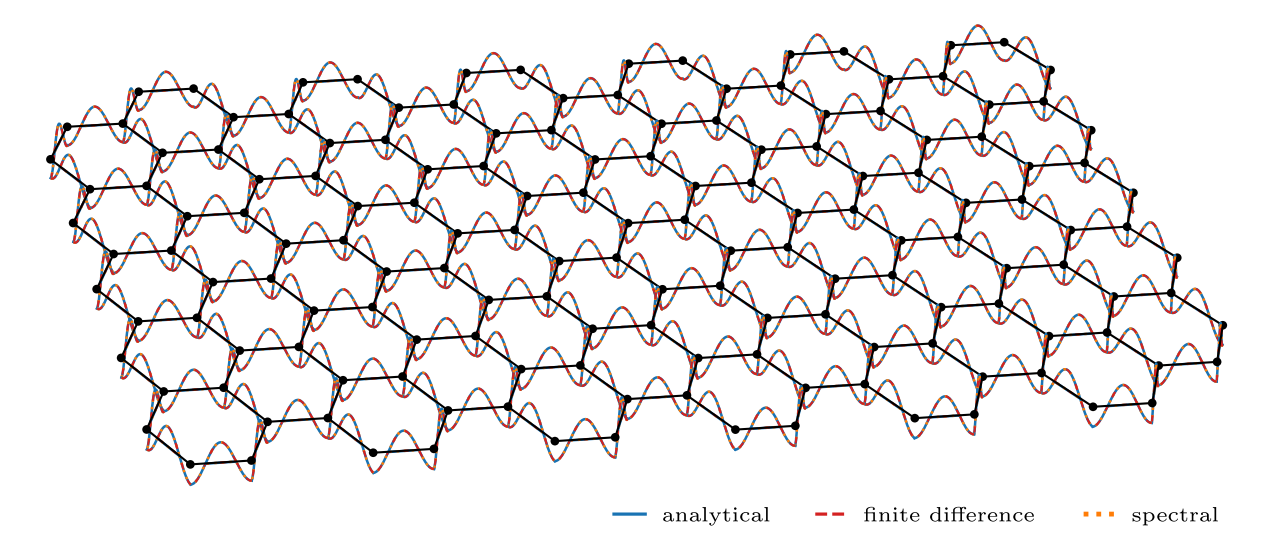


Figure 9. Solution of the Poisson equation (5.1) on a metric hexagonal lattice with N=154 nodes (black disks) and M=213 edges (black lines). All edges $i \in \{1,\ldots,M\}$ have length $\ell_i=1$ and Kirchhoff boundaries. The source term on the right-hand side of the Poisson equation is $\rho_i(x_i) = \cos(2\pi x_i)$ for each edge i. The solution (solid blue curve) of the Poisson equation is $\phi_i(x_i) = -\cos(2\pi x_i)/(4\pi^2)$ for each edge i. The dashed red and dotted orange curves indicate numerical solutions using finite-difference and spectral methods, respectively. These curves almost overlap the solid blue analytical solution and are practically indistinguishable at this scale.

the underlying Laplace–Kirchhoff matrices (3.11) and employ Eq. (3.13) to implement the Kirchhoff flux condition at the hub node, which is attached to all three edges.

In Figure 8(b), we show the numerical solutions for the 3-edge star network that we obtain using finite-difference and spectral methods. Both approaches are able to appropriately resolve the true solution.

As a second metric network, we consider a hexagonal lattice with N=154 nodes and M=213 edges [see Figure 9]. We set the lengths of all edges to 1, and we use $N_i=1000$ discretization intervals for all edges $i \in \{1, \ldots, 213\}$ in the finite-difference approach. We use the source term in Eq. (5.2). See our code repository [35] for the software implementation details for this example and all of our subsequent numerical examples. The numerical simulations from both the finite-difference and spectral approaches again closely resemble the analytical solution. Although we consider more than 200 edges and use 1000 finite-difference discretizations per edge, employing sparse-matrix solvers allows us to efficiently compute numerical solutions. In Appendix B, we consider metric hexagonal-lattice networks with up to about 10^4 nodes and about 10^4 edges.

As a third metric network, we examine a random-line network with N=8 nodes and M=10 edges [see Figure 10]. In a random-line network, one independently places line segments (i.e., "needles") of a specified length in a unit square (or other domain), forming an overlapping pattern [34]. Random-line networks, which are reminiscent of the Buffon-needle graphs that were considered in prior works on metric networks [42, 78], are a useful toy model to study PDEs on metric networks, as their edges are line segments of a specific length.

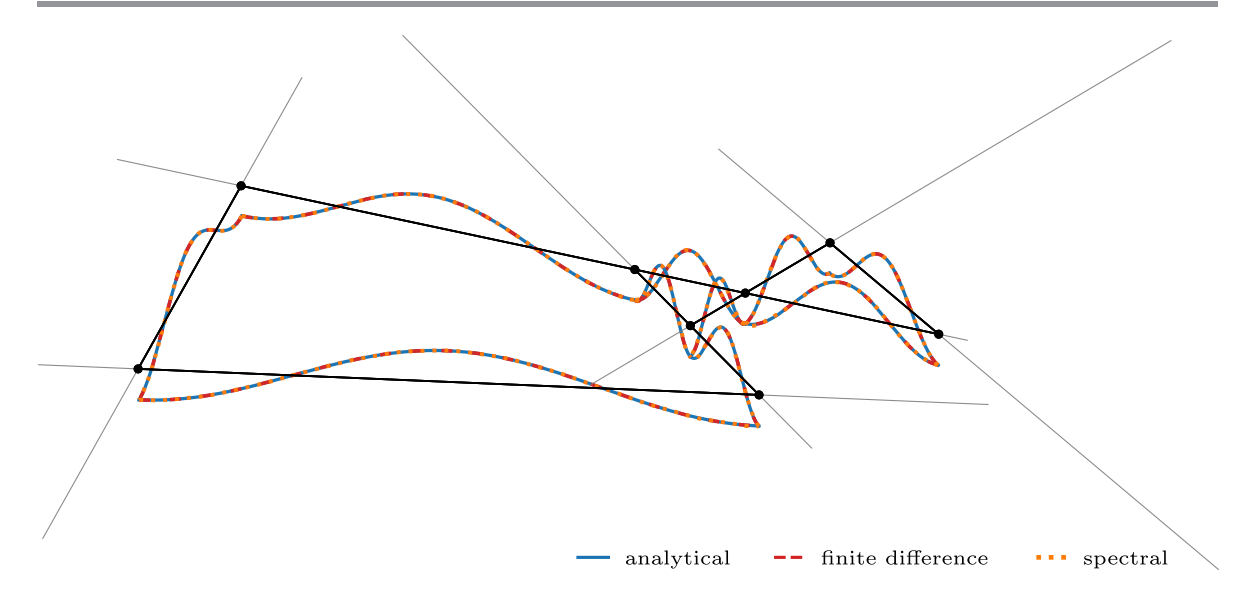


Figure 10. Solution of the Poisson equation (5.1) on a metric random-line network with N=8 nodes (black disks) and M=10 edges (black lines). In the depicted realization of a random-line network, we independently position six "needles" (gray line segments) of unit length in the unit square. (See [34] for further details about how to generate random-line networks.) All edges have Kirchhoff boundaries. The source term on the right-hand side of the Poisson equation is $\rho_i(x_i) = \cos(2\pi x_i/\ell_i)/\ell_i^2$ for each edge i. The solution (solid blue curve) of the Poisson equation is $\phi_i(x_i) = -\cos(2\pi x_i/\ell_i)/(4\pi^2)$ for each edge i. The dashed red and dotted orange curves indicate numerical solutions using finite-difference and spectral methods, respectively. These curves almost overlap the solid blue analytical solution and are practically indistinguishable at this scale.

Random-line networks and related spatial networks are relevant to the study of granular and particulate systems [141, 148, 182].

5.2. Heat equation. We now consider the inhomogeneous heat equation

$$\frac{\partial \phi}{\partial t} = \tilde{\Delta}\phi - \rho$$

with source term ρ . Its steady-state solutions satisfy the Poisson equation (5.1) in the limit as time $t \to \infty$.

In Figure 11(a), we show the solution of the heat equation (5.4) for our 3-edge star network. We set $\rho_i(x_i) = \cos(2\pi x_i)$ and $\phi_i(x_i, 0) = -3\cos(2\pi x_i)/(8\pi^2)$ for edges $i \in \{1, 2, 3\}$. For this initial condition and source term, $\lim_{t\to\infty} \phi_i(x_i, t) = -\cos(2\pi x_i)/(4\pi^2)$. In the supplementary material (M162815_01.mp4 [local/web 5.34MB]) [36], we show an animation of the solution $\phi(x,t)$ of Eq. (5.4) for both our 3-edge star network and the hexagonal lattice from Section 5.1.

5.3. Wave equation. As a final example of a PDE on a metric network, we study the wave equation

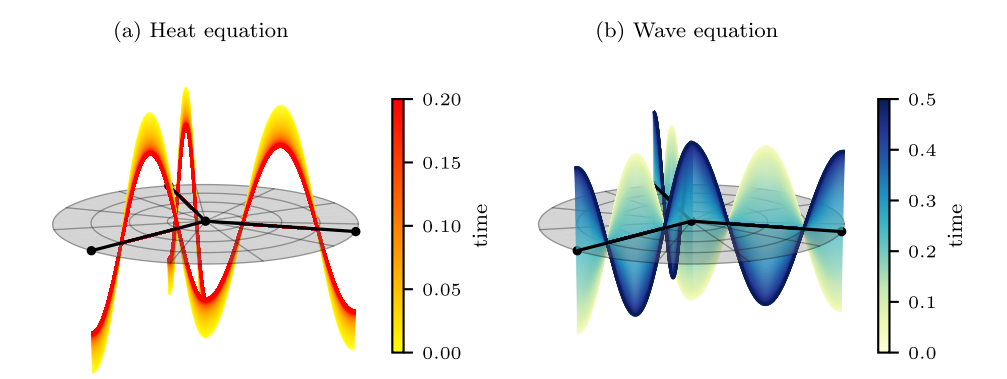


Figure 11. Solutions of the heat and wave equations on a metric star network with N=4 nodes (black disks) and M=3 edges (black lines). All edges $i \in \{1,2,3\}$ have length $\ell_i=1$ and Kirchhoff boundaries. (a) We consider the heat equation (5.4) with a source term $\rho_i(x_i) = \cos(2\pi x_i)$ and initial condition $\phi_i(x_i,0) = -3\cos(2\pi x_i)/(8\pi^2)$ for each edge i. In the limit as time $t \to \infty$, we recover the solution of the corresponding Poisson equation (i.e., $\lim_{t\to\infty}\phi_i(x_i,t) = -\cos(2\pi x_i)/(4\pi^2)$). (b) We consider the wave equation (5.5) with initial conditions $\phi_i(x_i,0) = -\cos(2\pi x_i)/(4\pi^2)$ and $\phi_i(x_i,0) = 0$ for each edge i. The solution is $\phi_i(x_i,t) = -[\cos(2\pi x_i)/(4\pi^2)]\cos(2\pi t)$ for each edge i. The depicted solutions use a finite-difference approach with $N_i = 1000$ discretizations per edge.

(5.5)
$$\frac{\partial^2 \phi}{\partial t^2} = \tilde{\Delta} \phi .$$

In Figure 11(b), we show the solution of the wave equation (5.5) for our 3-edge star network. For each edge $i \in \{1,2,3\}$, we set $\phi_i(x_i,0) = -\cos(2\pi x_i)/(4\pi^2)$ and $\dot{\phi}_i(x_i,0) = 0$. We thus obtain $\phi_i(x_i,t) = -[\cos(2\pi x_i)/(4\pi^2)]\cos(2\pi t)$ for each edge i. In the supplementary material (M162815_02.mp4 [local/web 8.45MB]) [37], we show an animation of the solution $\phi(x,t)$ of Eq. (5.5) for both our 3-edge star network and the hexagonal lattice from Section 5.1.

6. Conclusions and discussion. Metric networks give a mathematical framework to study spatially extended dynamics, such as partial differential equations, on networked systems [115]. Metric networks have applications in a variety of scientific fields, including in the investigation of the mechanical properties of materials [9, 19, 38, 85, 87, 90, 94], quantum dynamics in thin structures [4, 20, 22, 103, 104, 110, 111, 112, 157], information propagation in transmission lines [5, 47, 136, 137, 138, 139, 140, 150, 166], gas flow in pipelines [17, 43, 63, 64, 134], the spatiotemporal propagation of infectious diseases [109], and others.

Over the last three decades, the study of metric networks has progressed in parallel to (and largely independent of) developments in more conventional network science. In network science, the analysis of the interplay between network structure and dynamics has long been a key topic. Such research has used combinatorial networks, rather than metric networks, and accordingly it has focused primarily on ordinary differential equations and (both deterministic and stochastic) agent-based models on networks, rather than on PDEs. Augmenting the edges of a network by associating them with intervals with a metric structure yields a natural setting to analyze PDEs on networked systems. Unlike for combinatorial networks, dynamical processes on metric networks require one to specify continuity conditions and boundary conditions in addition to initial conditions. Both boundary conditions and network structure affect the eigenmodes of PDEs on metric networks.

In the present paper, we overviewed several approaches to study fundamental linear PDEs (the time-independent Schrödinger equation, the Poisson equation, the heat equation, and the wave equation) on metric networks. We expanded on the spectral approach in [42, 78] to account for degenerate eigenmodes and various algorithm inputs, including the range of characteristic wavenumbers, the rounding precision of potentially equivalent characteristic wavenumbers, and the optimization bounds (which determine the range of values over which one optimizes).

Although a spectral approach is useful to identify eigenmodes in a metric network, it can be challenging to accurately determine a large number of (potentially degenerate) eigenmodes to unambiguously determine the solution of a PDE. Visible deviations between Weyl's law and the characteristic-wavenumber counting function in a network with symmetries can arise from unresolved degenerate eigenmodes, and identifying symmetries and their corresponding degeneracies can help appropriately resolve all relevant eigenmodes in a metric network.

Complementing the numerical results of Brio et al. [42], who focused on systems involving the Poisson equation and the telegraph equation on a metric network with 3 edges, ¹² we studied the Poisson equation, the heat equation, and the wave equation on three distinct metric networks with much larger numbers of nodes and edges. The spectral solver, finite-difference solver, and visualization routines that we developed in our investigation are available at https://gitlab.com/ComputationalScience/metric-networks. A web application to listen to eigenmodes of the Schrödinger equation (3.1) on a metric star network with N=4 nodes, M=3 edges of potentially different lengths, and Kirchhoff boundary conditions is available at https://metricnets.streamlit.app/.

There are numerous worthwhile research directions to pursue in future work. Given the challenges of obtaining accurate solutions of different types of PDEs on metric networks, it is important to further develop and improve numerical solvers. For example, an algorithm that is based on the fast Fourier transform was proposed recently to solve PDEs on metric networks [44]. In addition to numerical techniques like finite-difference, finite-element, finite-volume, and spectral methods, potential approaches can also incorporate physics-informed neural networks (PINNs) [31], including ones that use spectral information [178]. In the spirit of [80], another promising avenue is extending symmetry arguments [16, 96] to various families of metric networks. The analysis of symmetries can yield important insights into how specific structural features influence eigenmodes and their degeneracies. For instance, for beam networks, Berkolaiko and Ettehad [21] used symmetry arguments and the quotient-graph method from [16] to perform efficient spectral analysis of a three-dimensional structure. It may also be worthwhile to explore connections between metric networks and systems such as the topological Dirac equation on networks and simplicial complexes [29]. Additionally, it is important to study nonlinear PDEs on large metric networks.

Code availability. Our code is publicly available at https://gitlab.com/Computational Science/metric-networks.

 $^{^{12}}$ Brio et al. [42] obtained solutions of PDEs on metric networks with 3 edges and 2 nodes, and they computed wavenumbers for metric networks with up to 165 edges and 104 nodes.

Appendix A. Symmetries. It is very important to consider symmetries to understand dynamical processes on networks [80]. In this appendix, we illustrate how to use symmetry groups [40, 66, 175, 180] to identify degeneracies in the eigenmodes of PDEs on metric networks. To do this, one first determines the irreducible representations of a symmetry group, and one then determines eigenmode degeneracies by considering the dimensions of the associated irreducible representations. Such group-theoretic approaches can help one assess whether or not a numerical method has successfully identified all of the eigenmodes in a metric network.

Degenerate eigenmodes, such as the ones in Eq. (4.5), are usually associated with a symmetry of a metric network. For example, in our 3-edge star network (see Figure 5), we obtain the same characteristic wavenumbers and corresponding eigenmodes of a PDE if we permute the three identical length- ℓ edges, which have the same function space and the same operator space. In this example, the relevant symmetry group is the symmetric group S_3 , which consists of the $|S_3| = 3! = 6$ possible permutations of the elements of the set $\{1,2,3\}$. Using cycle notation,¹³ the set of elements of S_3 is $\{1,(1,2),(2,3),(1,3),(1,2,3),(1,3,2)\}$, where 1 is the identity element. Permutations that involve two elements are called "transpositions", and permutations that involve three elements are called "3-cycles". The three distinct types of cycle structures in S_3 yield C=3 conjugacy classes, which are relevant for characterizing degenerate eigenmodes.

Consider the permutation representation $P: S_3 \to GL(\mathbb{R}^3)$ of S_3 , where GL(V) denotes the general linear group of automorphisms of a vector space V. The space V is \mathbb{R}^3 , and the edges e_1 , e_2 , and e_3 are represented by the vectors

(A.1)
$$e_1 = \begin{pmatrix} 1 \\ 0 \\ 0 \end{pmatrix}, \quad e_2 = \begin{pmatrix} 0 \\ 1 \\ 0 \end{pmatrix}, \quad e_3 = \begin{pmatrix} 0 \\ 0 \\ 1 \end{pmatrix}.$$

In this representation, the permutation $\pi = (1,2,3)$ is

(A.2)
$$P(\pi) = \begin{pmatrix} 0 & 0 & 1 \\ 1 & 0 & 0 \\ 0 & 1 & 0 \end{pmatrix}.$$

Observe that $P(\pi)e_1 = e_2$, $P(\pi)e_2 = e_3$, and $P(\pi)e_3 = e_1$. One can similarly determine matrix representations of the remaining five elements of the group S_3 .

Given a representation P, the character $\chi^{(P)}: S_3 \to \mathbb{R}$ assigns the trace of the corresponding matrix representation to each group element $g \in S_3$. That is,

(A.3)
$$\chi^{(P)}(g) = \operatorname{tr}(P(g)).$$

For the three conjugacy classes of S_3 and the permutation representation P, the corresponding characters are $\chi_1^{(P)} = 3$ (the identity permutation, in which no elements are rearranged),

 $^{^{13}}$ In cycle notation, one describes a permutation as a product of disjoint cycles [180]. In each cycle (*i.e.*, cyclic permutation), one rearranges a set of elements. For example, the cyclic permutation (1,2,3) maps 1 to 2, 2 to 3, and 3 to 1.

 $\chi_2^{(P)} = 1$ (the transpositions, in which two elements are swapped and one element remains in its current position), and $\chi_3^{(P)} = 0$ (the 3-cycles, in which no elements remain in their current positions).

A representation P is "semisimple" (i.e., completely reducible) if one can decompose it into a direct sum of irreducible representations $P^{(\alpha)}$. That is,

(A.4)
$$P = \bigoplus_{\alpha=1}^{C} c_{\alpha} P^{(\alpha)},$$

where C is the number of conjugacy classes and the coefficient c_{α} is an integer that encodes the number of times that $P^{(\alpha)}$ appears in the decomposition (A.4). Taking the trace of Eq. (A.4) yields

(A.5)
$$\chi^{(P)}(g) = \sum_{\alpha=1}^{C} c_{\alpha} \chi^{(\alpha)}(g).$$

The dimensions d_{α} of the irreducible representations $P^{(\alpha)}$ of a finite group G satisfy

(A.6)
$$\sum_{\alpha=1}^{C} d_{\alpha}^{2} = |G|.$$

For the group S_3 , the only dimensions of the three irreducible representations that satisfy $d_1^2 + d_2^2 + d_3^2 = 6$ are $d_1 = d_2 = 1$ and $d_3 = 2$. The two one-dimensional irreducible representations correspond to the trivial and sign representations. In the trivial representation, one maps each element of S_3 to 1. In the sign representation, one maps each permutation to its corresponding sign, which is 1 for even permutations and -1 for odd permutations. According to Shur's lemma (see Lemma A.1), the two-dimensional irreducible representation leads to the eigenmode degeneracy that we observed in Section 4. This representation is the "standard representation" of S_3 . It is a "faithful" representation, which means that it gives a one-to-one mapping of group elements to their corresponding matrices. By contrast, the other two representations are not faithful.

A representation P of a finite group G is irreducible if and only if

(A.7)
$$\sum_{\alpha=1}^{C} n_{\alpha} |\chi_{\alpha}^{(P)}|^{2} = |G|,$$

where n_{α} denotes the number of elements in the α th conjugacy class. For a reducible representation,

(A.8)
$$\sum_{\alpha=1}^{C} n_{\alpha} |\chi_{\alpha}^{(P)}|^{2} > |G|.$$

Inserting the values of n_{α} and $\chi_{\alpha}^{(P)}$ that are associated with the permutation representation yields

(A.9)
$$\sum_{\alpha=1}^{C} n_{\alpha} |\chi_{\alpha}^{(P)}|^{2} = 1 \times 3^{2} + 3 \times 1^{2} + 2 \times 0^{2} = 12.$$

Table 2 Character table of the symmetric group S_3 .

	1	(1, 2)	(1, 2, 3)
trivial representation	1	1	1
sign representation	1	-1	1
standard representation	2	0	-1

Because $12 > |S_3| = 6$, the permutation representation is reducible. The decomposition coefficients c_{α} [see Eq. (A.4)] are

(A.10)
$$c_{\alpha} = \frac{1}{|G|} \sum_{\beta=1}^{C} n_{\beta} \chi_{\beta}^{(P)} (\chi_{\beta}^{(\alpha)})^{*},$$

where the superscript * denotes complex conjugation and $\chi_{\beta}^{(\alpha)}$ denotes the value of the character $\chi^{(\alpha)}$ of the irreducible representation $P^{(\alpha)}$ on the β th conjugacy class of the group G. Using the character table (see Table 2) yields

(A.11)
$$c_1 = \frac{1}{6} (1 \times 3 \times 1 + 3 \times 1 \times 1 + 2 \times 0 \times 1) = 1$$

(A.11)
$$c_1 = \frac{1}{6} (1 \times 3 \times 1 + 3 \times 1 \times 1 + 2 \times 0 \times 1) = 1,$$
(A.12)
$$c_2 = \frac{1}{6} (1 \times 3 \times 1 + 3 \times 1 \times (-1) + 2 \times 0 \times 1) = 0,$$

(A.13)
$$c_3 = \frac{1}{6} (1 \times 3 \times 2 + 3 \times 1 \times 0 + 2 \times 0 \times (-1)) = 1.$$

We can thus decompose the permutation representation P of the symmetric group S_3 as

(A.14)
$$P = P^{(1)} \oplus P^{(3)}.$$

That is, the permutation representation P of the symmetric group S_3 is the direct sum of the trivial irreducible representation $P^{(1)}$ and the two-dimensional irreducible representation $P^{(3)}$

For the linear time-independent Schrödinger equation on the 3-edge metric star network (see Section 4), the characteristic wavenumbers and eigenmodes that are associated with the Hamiltonian $\mathcal{H} = -\hat{\Delta}$ (i.e., the generalized negative Laplacian that includes continuity and boundary conditions) are invariant with respect to permutations of the edges. That is, the permutation operator P commutes with \mathcal{H} (i.e., $[\mathcal{H}, P] = 0$), so

(A.15)
$$\widetilde{\mathcal{H}}Pf = P\widetilde{\mathcal{H}}f = -Pk^2f = -k^2Pf.$$

We now choose a basis so that the permutation operator decomposes into a direct sum of the irreducible representations $P^{(1)}$ and $P^{(3)}$. By Schur's lemma, the Hamiltonian $\widetilde{\mathcal{H}}$ becomes diagonal in this basis.

Lemma A.1 (Schur's lemma). If $P: G \to \operatorname{GL}(V)$ is an irreducible representation of a finite group G and there exists a matrix E that commutes with every element $q \in G$ (i.e., EP(g) = P(g)E for all $g \in G$), then $E = \lambda I$, where I is the identity matrix and $\lambda \in \mathbb{C}$.

According to Schur's lemma, in the basis in which the representation P decomposes into irreducible representations $P^{(1)}$ and $P^{(3)}$, the basis vectors are eigenstates (*i.e.*, eigenfunctions) of the Hamiltonian $\widetilde{\mathcal{H}}$. The dimensions $d_1 = 1$ and $d_3 = 2$ of these irreducible representations correspond to the degeneracies that we observed in solutions of PDEs on the metric star network with 3 length- ℓ edges [40, 146, 180].

One can also interpret the symmetries of a network by decomposing the network into simpler substructures (so-called "quotient graphs") that reproduce the spectrum of the entire network [16]. For the metric star network with 3 length- ℓ edges, the trivial representation (whose irreducible representation has dimension $d_1 = 1$) results in one interval $[0, \ell]$ with Kirchhoff boundary conditions at both ends. By contrast, the standard representation (whose irreducible representation has dimension $d_3 = 2$) is associated with two intervals $[0, \ell]$ that each have a Kirchhoff boundary condition at one end and a Dirichlet boundary condition at the other end. The sign representation corresponds to a network with 0 nodes. Ježek and Lipovský [96] studied this decomposition using the theory of symmetry operations on metric networks that was developed by Band et al. [16].

We now apply the arguments that we presented for the symmetry group S_3 to a metric star network with four length- ℓ edges. Without explicitly calculating the characteristic wavenumbers and eigenmodes of a PDE, we deduce the underlying degeneracies by examining the irreducible representations that are associated with the permutation representation of S_4 . A similar calculation as with S_3 shows that the permutation representation of S_4 is the direct sum of the one-dimensional trivial representation and the three-dimensional standard representation. Therefore, the eigenmode degeneracies are 1 and 3. Indeed, an explicit calculation of the determinant of the coupling-condition matrix $T_+(k_m)$ [see Eq. (3.4)] for this 4-edge star network yields $\det(T_+(k_m)) = 4\cos(k_m\ell)^3\sin(k_m\ell)$, 14 demonstrating that the group-theoretically determined degeneracies coincide with the degeneracies that one obtains by calculating the determinant of $T_+(k_m)$.

In summary, when using a group-theoretic approach to determine eigenmode degeneracies for the Schrödinger equation on a metric network (and, more generally, to determine the eigenstate degeneracies for a Hamiltonian that is associated with a metric network), we follow the following procedure:

- Given a metric network, determine the characters of a representation of the largest (i.e., full) symmetry group that acts on the network.
- Calculate the decomposition coefficients c_{α} [see Eq. (A.10)] and the corresponding decomposition into irreducible representations [see Eq. (A.4)]. The dimensions of the irreducible representations with nonzero coefficients c_{α} are equal to the degeneracies of the system's eigenstates.

It is possible for accidental degeneracies to result in equal eigenvalues that correspond to different irreducible representations [24, 130]. This caveat notwithstanding, degeneracies in

¹⁴The determinant of the coupling-condition matrix for an M-edge metric star network with edges $i \in \{1,\ldots,M\}$ of length ℓ_i is $\det(T(k_m)) = \sum_{i=1}^M \tan(k_m \ell_i) \prod_{i=1}^M \cos(k_m \ell_i)$ [147]. Unlike in the coupling-condition matrices for the 3-edge and 4-edge star networks, we use the notation T without a subscript for simplicity.

¹⁵Analogously to the notation T_{λ} in Section 4, we use T_{+} (with a 4-pointed star as a subscript) to denote the coupling-condition matrix [see Eq. (3.4)] that is associated with the 4-edge star network with Kirchhoff flux conditions.

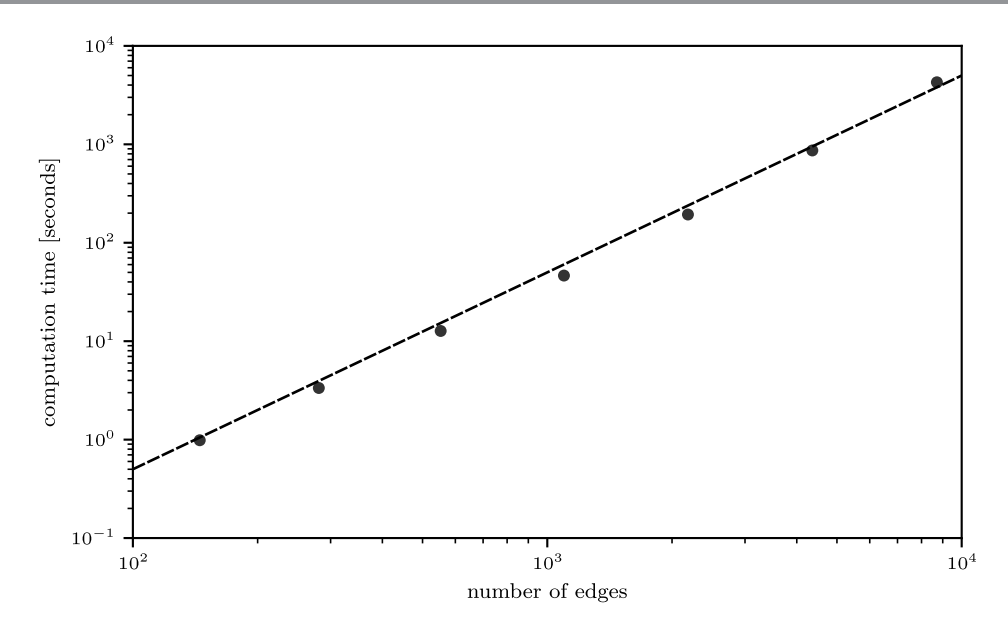


Figure 12. Computation time for solving the Poisson equation (5.1) on metric hexagonal-lattice networks with a finite-difference approach for different numbers N of nodes and numbers M of edges: $(N, M) \in \{(106, 145), (202, 281), (394, 553), (778, 1097), (1546, 2185), (3082, 4361), (6154, 8713)\}$. All edges $i \in \{1, ..., M\}$ have length $\ell_i = 1$ and Kirchhoff boundaries. The source term on the right-hand side of the Poisson equation (5.1) is $\rho_i(x_i) = \cos(2\pi x_i)$ for each edge. The solution of the Poisson equation is $\phi_i(x_i) = -\cos(2\pi x_i)/(4\pi^2)$ for each edge. The dashed black line corresponds to a power law with exponent 2.

the eigenvalues of a PDE on a metric network are usually associated with the symmetries of the metric network. One can use small perturbations of the edge lengths of a metric network to break symmetries [23, 76]. For the Schrödinger equation on a metric network with Kirchhoff boundary conditions, the eigenvalues are usually simple (*i.e.*, their algebraic multiplicity is usually 1) [52, 76]. Nevertheless, given the broad relevance of symmetric network structures, it is important to consider the connections between symmetry groups and eigenmode degeneracies.

Appendix B. Large networks. We numerically solve the Poisson equation (5.1) on metric hexagonal-lattice networks with different numbers of nodes and edges. The source term is given by Eq. (5.2). The length ℓ_i of each edge $i \in \{1, ..., M\}$ is 1, and all boundaries are of Kirchhoff type. The solution of the corresponding Poisson equation is $\phi_i(x_i) = -\cos(2\pi x_i)/(4\pi^2)$.

To solve the Poisson equation on these metric networks, we employ a finite-difference approach and set the number of discretization intervals to $N_i = 1000$ for all edges. In Figure 12, we show the computation time as a function of the number of edges in these metric networks. The largest metric network that we consider has 6154 nodes and 8713 edges. Solving the Poisson equation on this network takes about 4300 seconds (i.e., about 1.2 hours) on one i7 CPU core with a 1.8 GHz clock speed. In all of our simulations, the mean-squared error between the numerical and analytical solutions is less than 10^{-17} . For this error calculation, we use vectors that encode discretized solutions of the Poisson equation at all edges.

Acknowledgments. We thank the participants — especially Gregory Berkolaiko, Jean-Guy Caputo, Pia Domschke, Christina Durón, Hannah Kravitz, Stefan Le Coz, and Jeremy Marzuola — of the 2024 metric-networks workshop at the Frankfurt School of Finance and Management for their valuable feedback. We also thank Justin Curry, Roy Goodman, Eric Hester, Kye Shi, and the two anonymous referees for helpful comments. MAP thanks Leonid Bunimovich for introducing him to quantum graphs more than 20 years ago. It has taken a long time, but that introduction created the initial kernel that has finally led to the present paper.

REFERENCES

- M. J. ABLOWITZ AND J. F. LADIK, Nonlinear differential-difference equations, J. Math. Phys., 16 (1975), pp. 598-603, https://doi.org/10.1063/1.522558.
- [2] M. J. Ablowitz and J. F. Ladik, Nonlinear differential-difference equations and Fourier analysis, J. Math. Phys., 17 (1976), pp. 1011-1018, https://doi.org/10.1063/1.523009.
- [3] R. Albert, H. Jeong, and A.-L. Barabási, Error and attack tolerance of complex networks, Nature, 406 (2000), pp. 378–382, https://doi.org/10.1038/35019019.
- [4] S. Alexander, Superconductivity of networks. A percolation approach to the effects of disorder, Phys. Rev. B, 27 (1983), pp. 1541–1557, https://doi.org/10.1103/PhysRevB.27.1541.
- [5] P. Alonso Ruiz, Power dissipation in fractal Feynman–Sierpinski AC circuits, J. Math. Phys., 58 (2017), 073503, https://doi.org/10.1063/1.4994197.
- [6] F. M. Andrade, A. G. M. Schmidt, E. Vicentini, B. K. Cheng, and M. G. E. da Luz, Green's function approach for quantum graphs: An overview, Phys. Rep., 647 (2016), pp. 1–46, https://doi. org/10.1016/j.physrep.2016.07.001.
- [7] W. Arendt, R. Nittka, W. Peter, and F. Steiner, Weyl's Law: Spectral Properties of the Laplacian in Mathematics and Physics, John Wiley & Sons, Hoboken, NJ, USA, 2009.
- [8] M. ARIOLI AND M. BENZI, A finite element method for quantum graphs, IMA J. Numer. Anal., 38 (2018), pp. 1119–1163, https://doi.org/10.1093/imanum/drx029.
- [9] W. T. ASHURST AND W. G. HOOVER, Microscopic fracture studies in the two-dimensional triangular lattice, Phys. Rev. B, 14 (1976), pp. 1465–1473, https://doi.org/10.1103/PhysRevB.14.1465.
- [10] M. ASLLANI, D. M. BUSIELLO, T. CARLETTI, D. FANELLI, AND G. PLANCHON, Turing patterns in multiplex networks, Phys. Rev. E, 90 (2014), 042814, https://doi.org/10.1103/PhysRevE.90.042814.
- [11] M. ASLLANI, D. M. BUSIELLO, T. CARLETTI, D. FANELLI, AND G. PLANCHON, Turing instabilities on Cartesian product networks, Sci. Rep., 5 (2015), 12927, https://doi.org/10.1038/srep12927.
- [12] A. R. Atilgan, S. R. Durell, R. L. Jernigan, M. C. Demirel, O. Keskin, and I. Bahar, Anisotropy of fluctuation dynamics of proteins with an elastic network model, Biophys. J., 80 (2001), pp. 505–515, https://doi.org/10.1016/S0006-3495(01)76033-X.
- [13] G. AULETTA, M. FORTUNATO, AND G. PARISI, *Quantum Mechanics*, Cambridge University Press, Cambridge, UK, 2012.
- [14] S. A. AVDONIN, A. S. MIKHAYLOV, V. S. MIKHAYLOV, AND A. E. CHOQUE-RIVERO, Discretization of the wave equation on a metric graph, Math. Methods Appl. Sci., 48 (2025), pp. 5708–5717, https://doi.org/10.1002/mma.10630.
- [15] I. Bahar, A. R. Atilgan, and B. Erman, Direct evaluation of thermal fluctuations in proteins using a single-parameter harmonic potential, Folding and Design, 2 (1997), pp. 173–181, https://doi.org/10.1016/S1359-0278(97)00024-2.
- [16] R. Band, G. Berkolaiko, C. H. Joyner, and W. Liu, Quotients of graph operators by symmetry representations, preprint, arXiv:1711.00918, 2017.
- [17] M. K. BANDA, M. HERTY, AND A. KLAR, Gas flow in pipeline networks, Netw. Heterog. Media, 1 (2006), pp. 41–56, https://doi.org/10.3934/nhm.2006.1.41.
- [18] F. BARRA AND P. GASPARD, On the level spacing distribution in quantum graphs, J. Stat. Phys., 101 (2000), pp. 283–319, https://doi.org/10.1023/A:1026495012522.
- [19] P. D. Beale and D. J. Srolovitz, Elastic fracture in random materials, Phys. Rev. B, 37 (1988), pp. 5500–5507, https://doi.org/10.1103/PhysRevB.37.5500.

- [20] G. Berkolaiko, An elementary introduction to quantum graphs, in Geometric and Computational Spectral Theory, A. Girouard, D. Jakobson, M. Levitin, N. Nigam, I. Polterovich, and F. Rochon, eds., American Mathematical Society, Providence, RI, USA, 2017, pp. 41–72, https://doi.org/10.1090/conm/700.
- [21] G. BERKOLAIKO AND M. ETTEHAD, Three-dimensional elastic beam frames: Rigid joint conditions in variational and differential formulation, Stud. Appl. Math., 148 (2022), pp. 1586–1623, https://doi.org/10.1111/sapm.12485.
- [22] G. BERKOLAIKO AND P. KUCHMENT, Introduction to Quantum Graphs, American Mathematical Society, Providence, RI, USA, 2013.
- [23] G. BERKOLAIKO AND W. LIU, Simplicity of eigenvalues and non-vanishing of eigenfunctions of a quantum graph, J. Math. Anal. Appl., 445 (2017), pp. 803–818, https://doi.org/10.1016/j.jmaa.2016.07.026.
- [24] G. Berkolaiko and W. Liu, Eigenspaces of symmetric graphs are not typically irreducible, Lett. Math. Phys., 108 (2018), pp. 1825–1835, https://doi.org/10.1007/s11005-018-1050-7.
- [25] W. BERNARDONI, R. CARDONA, J. CLEVELAND, J. CURRY, R. GREEN, B. HELLER, A. HYLTON, T. LAM, AND R. KASSOUF-SHORT, Algebraic and geometric models for space networking, preprint, arXiv:2304.01150, 2023.
- [26] E. Berthier, M. A. Porter, and K. E. Daniels, Forecasting failure locations in 2-dimensional disordered lattices, Proc. Natl. Acad. Sci. USA, 116 (2019), pp. 16742–16749.
- [27] C. Besse, R. Duboscq, and S. Le Coz, Numerical simulations on nonlinear quantum graphs with the GrafiDi library, SMAI J. Comput. Math., 8 (2022), pp. 1–47, https://doi.org/10.5802/smai-jcm.78.
- [28] M. BIAŁOUS, V. YUNKO, S. BAUCH, M. LAWNICZAK, B. DIETZ, AND L. SIRKO, Power spectrum analysis and missing level statistics of microwave graphs with violated time reversal invariance, Phys. Rev. Lett., 117 (2016), 144101, https://doi.org/10.1103/PhysRevLett.117.144101.
- [29] G. BIANCONI, The topological Dirac equation of networks and simplicial complexes, J. Phys. Complexity, 2 (2021), 035022, https://doi.org/10.1088/2632-072X/ac19be.
- [30] C. Bick, E. Gross, H. A. Harrington, and M. T. Schaub, What are higher-order networks?, SIAM Rev., 65 (2023), pp. 686–731, https://doi.org/10.1137/21M1414024.
- [31] J. Blechschmidt, J.-F. Pietschman, T.-C. Riemer, M. Stoll, and M. Winkler, A comparison of PINN approaches for drift-diffusion equations on metric graphs, preprint, arXiv:2205.07195, 2022.
- [32] D. Bolin, A. B. Simas, and J. Wallin, Gaussian Whittle-Matérn fields on metric graphs, preprint, arXiv:2205.06163, 2022.
- [33] D. Bonamy and E. Bouchaud, Failure of heterogeneous materials: A dynamic phase transition?, Phys. Rep., 498 (2011), pp. 1–44, https://doi.org/10.1016/j.physrep.2010.07.006.
- [34] L. BÖTTCHER, A random-line-graph approach to overlapping line segments, J. Complex Networks, 8 (2020), cnaa029, https://doi.org/10.1093/comnet/cnaa029.
- [35] L. BÖTTCHER, GitLab Repository, https://gitlab.com/ComputationalScience/metric-networks, 2023.
- [36] L. BÖTTCHER, The Heat Equation on Metric Networks, https://vimeo.com/898777272, 2023.
- [37] L. BÖTTCHER, The Wave Equation on Metric Networks, https://vimeo.com/898776782, 2023.
- [38] L. BÖTTCHER AND H. J. HERRMANN, Computational Statistical Physics, Cambridge University Press, Cambridge, UK, 2021, https://doi.org/10.1017/9781108882316.
- [39] L. BÖTTCHER, J. NAGLER, AND H. J. HERRMANN, Critical behaviors in contagion dynamics, Phys. Rev. Lett., 118 (2017), 088301, https://doi.org/10.1103/PhysRevLett.118.088301.
- [40] V. BOUCHARD, Group Theory in Physics: Lecture Notes, 2020, https://sites.ualberta.ca/~vbouchar/ MAPH464/notes.html, last accessed 4 September 2023.
- [41] R. P. Brent, Algorithms for Minimization Without Derivatives, Courier Corporation, Chelmsford, MA, USA, 2013.
- [42] M. Brio, J.-G. Caputo, and H. Kravitz, Spectral solutions of PDEs on networks, Appl. Numer. Math., 172 (2022), pp. 99–117, https://doi.org/10.1016/j.apnum.2021.09.021.
- [43] J. Brouwer, I. Gasser, and M. Herty, Gas pipeline models revisited: Model hierarchies, nonisothermal models, and simulations of networks, Multiscale Model. Simul., 9 (2011), pp. 601–623, https://doi.org/10.1137/100813580.
- [44] R. CARLSON, A quantum graph FFT with applications to partial differential equations on networks, preprint, arXiv:2410.19969, 2024.
- [45] M. CAVALCANTE, The Korteweg-de Vries equation on a metric star graph, Z. Angew. Math. Phys., 69 (2018), 124, https://doi.org/10.1007/s00033-018-1018-6.

- [46] J. Che, X. Zhang, W. Zhang, B. Dietz, and G. Chai, Fluctuation properties of the eigenfrequencies and scattering matrix of closed and open unidirectional graphs with chaotic wave dynamics, Phys. Rev. E, 106 (2022), 014211, https://doi.org/10.1103/PhysRevE.106.014211.
- [47] J. P. Chen, L. G. Rogers, L. Anderson, U. Andrews, A. Brzoska, A. Coffey, H. Davis, L. Fisher, M. Hansalik, S. Loew, and A. Teplyaev, Power dissipation in fractal AC circuits, J. Phys. A, 50 (2017), 325205, https://doi.org/10.1088/1751-8121/aa7a66.
- [48] B. V. Chirikov, A universal instability of many-dimensional oscillator systems, Phys. Rep., 52 (1979), pp. 263–379, https://doi.org/10.1016/0370-1573(79)90023-1.
- [49] F. CHUNG AND S.-T. YAU, Discrete Green's functions, J. Combin. Theory Ser. A, 91 (2000), pp. 191–214, https://doi.org/10.1006/jcta.2000.3094.
- [50] R. COHEN, K. EREZ, D. BEN-AVRAHAM, AND S. HAVLIN, Resilience of the internet to random break-downs, Phys. Rev. Lett., 85 (2000), pp. 4626–4628, https://doi.org/10.1103/PhysRevLett.85.4626.
- [51] R. COHEN, K. EREZ, D. BEN-AVRAHAM, AND S. HAVLIN, Breakdown of the internet under intentional attack, Phys. Rev. Lett., 86 (2001), pp. 3682–3685, https://doi.org/10.1103/PhysRevLett.86.3682.
- [52] Y. COLIN DE VERDIÈRE, Semi-classical measures on quantum graphs and the Gauß map of the determinant manifold, Ann. Henri Poincaré, 16 (2015), pp. 347–364, https://doi.org/10.1007/s00023-014-0326-4.
- [53] Q. Cui and I. Bahar, Normal Mode Analysis: Theory and Applications to Biological and Chemical Systems, CRC Press, Boca Raton, FL, USA, 2005.
- [54] L. DANON, T. A. HOUSE, J. M. READ, AND M. J. KEELING, Social encounter networks: Collective properties and disease transmission, J. R. Soc. Interface, 9 (2012), pp. 2826–2833, https://doi.org/ 10.1098/rsif.2012.0357.
- [55] L. DANON, J. M. READ, T. A. HOUSE, M. C. VERNON, AND M. J. KEELING, Social encounter networks: Characterizing Great Britain, Proc. Roy. Soc. B: Biol. Sci., 280 (2013), 20131037, https://doi.org/10.1098/rspb.2013.1037.
- [56] C. D'APICE, S. GÖTTLICH, M. HERTY, AND B. PICCOLI, Modeling, Simulation, and Optimization of Supply Chains: A Continuous Approach, SIAM, Philadelphia, PA, USA, 2010, https://doi.org/10.1137/1.9780898717600.
- [57] T. DAUXOIS, M. PEYRARD, AND S. RUFFO, The Fermi-Pasta-Ulam "numerical experiment": History and pedagogical perspectives, Eur. J. Phys., 26 (2005), pp. S3-S11, https://doi.org/10.1088/0143-0807/26/ 5/S01.
- [58] E. B. DAVIES, P. EXNER, AND J. LIPOVSKÝ, Non-Weyl asymptotics for quantum graphs with general coupling conditions, J. Phys. A, 43 (2010), 474013, https://doi.org/10.1088/1751-8113/43/47/474013.
- [59] E. B. Davies and A. Pushnitski, Non-Weyl resonance asymptotics for quantum graphs, Anal. PDE, 4 (2012), pp. 729–756, https://doi.org/10.2140/apde.2011.4.729.
- [60] L. DE ARCANGELIS, S. REDNER, AND A. CONIGLIO, Anomalous voltage distribution of random resistor networks and a new model for the backbone at the percolation threshold, Phys. Rev. B, 31 (1985), pp. 4725–4727, https://doi.org/10.1103/PhysRevB.31.4725.
- [61] B. Dekoninck and S. Nicaise, *The eigenvalue problem for networks of beams*, Linear Algebra Appl., 314 (2000), pp. 165–189, https://doi.org/10.1016/S0024-3795(00)00118-X.
- [62] B. Dietz, T. Klaus, M. Masi, M. Miski-Oglu, A. Richter, T. Skipa, and M. Wunderle, Closed and open superconducting microwave waveguide networks as a model for quantum graphs, Phys. Rev. E, 109 (2024), 034201, https://doi.org/10.1103/PhysRevE.109.034201.
- [63] P. Domschke, B. Geissler, O. Kolb, J. Lang, A. Martin, and A. Morsi, Combination of nonlinear and linear optimization of transient gas networks, INFORMS J. Comput., 23 (2011), pp. 605–617, https://doi.org/10.1287/ijoc.1100.0429.
- [64] P. Domschke, B. Hiller, J. Lang, V. Mehrmann, R. Morandin, and C. Tischendorf, Gas Network Modeling: An Overview (extended English version), TRR 154, Technische Universität Darmstadt, 2021, https://opus4.kobv.de/opus4-trr154/frontdoor/index/index/docId/411, last accessed 30 July 2025.
- [65] P. DORUKER, A. R. ATILGAN, AND I. BAHAR, Dynamics of proteins predicted by molecular dynamics simulations and analytical approaches: Application to α-amylase inhibitor, Proteins: Structure, Function, and Bioinformatics, 40 (2000), pp. 512–524, https://doi.org/10.1002/1097-0134(20000815)40: 3%3C512::AID-PROT180%3E3.0.CO;2-M.

- [66] M. S. Dresselhaus, G. Dresselhaus, and A. Jorio, Group Theory: Application to the Physics of Condensed Matter, Springer-Verlag, Heidelberg, Germany, 2007.
- [67] R. M. D'SOUZA, J. GÓMEZ-GARDENES, J. NAGLER, AND A. ARENAS, Explosive phenomena in complex networks, Adv. Phys., 68 (2019), pp. 123–223, https://doi.org/10.1080/00018732.2019.1650450.
- [68] L. C. Evans, Partial Differential Equations, 2nd ed., American Mathematical Society, Providence, RI, USA, 2010.
- [69] E. Fermi, J. Pasta, S. Ulam, and M. Tsingou, Studies of Nonlinear Problems. I, Technical report, Los Alamos National Laboratory (LANL), Los Alamos, NM, Report LA-1940, 1955.
- [70] R. P. FEYNMAN, R. B. LEIGHTON, AND M. SANDS, Feynman Lectures on Physics, Volume II: Mainly Electromagnetism and Matter, Addison-Wesley Publishing Company, Reading, MA, USA, 1966.
- [71] S. Flach and A. V. Gorbach, Discrete breathers Advances in theory and applications, Phys. Rep., 467 (2008), pp. 1–116, https://doi.org/10.1016/j.physrep.2008.05.002.
- [72] A. FLACHE, M. MÄS, T. FELICIANI, E. CHATTOE-BROWN, G. DEFFUANT, S. HUET, AND J. LORENZ, Models of social influence: Towards the next frontiers, J. Artif. Soc. Soc. Simul., 20 (2017), 2, https://doi.org/10.18564/jasss.3521.
- [73] H. FLASCHKA, On the Toda lattice. II: Inverse-scattering solution, Progr. Theoret. Phys., 51 (1974), pp. 703-716, https://doi.org/10.1143/PTP.51.703.
- [74] H. FLASCHKA, The Toda lattice. II. Existence of integrals, Phys. Rev. B, 9 (1974), pp. 1924–1925, https://doi.org/10.1103/PhysRevB.9.1924.
- [75] A. FORROW, F. G. WOODHOUSE, AND J. DUNKEL, Functional control of network dynamics using designed Laplacian spectra, Phys. Rev. X, 8 (2018), 041043, https://doi.org/10.1103/PhysRevX.8.041043.
- [76] L. FRIEDLANDER, Genericity of simple eigenvalues for a metric graph, Israel J. Math., 146 (2005), pp. 149–156, https://doi.org/10.1007/BF02773531.
- [77] J. FRIEDMAN AND J.-P. TILLICH, Wave equations for graphs and the edge-based Laplacian, Pac. J. Math., 216 (2004), pp. 229–266, https://doi.org/10.2140/pjm.2004.216.229.
- [78] M. GAIO, D. SAXENA, J. BERTOLOTTI, D. PISIGNANO, A. CAMPOSEO, AND R. SAPIENZA, *A nanophotonic laser on a graph*, Nat. Commun., 10 (2019), 226, https://doi.org/10.1038/s41467-018-08132-7.
- [79] L. G. GAJEWSKI, J. SIENKIEWICZ, AND J. A. HOLYST, Discovering hidden layers in quantum graphs, Phys. Rev. E, 104 (2021), 034311, https://doi.org/10.1103/PhysRevE.104.034311.
- [80] M. GOLUBITSKY AND I. STEWART, Dynamics and Bifurcation in Networks: Theory and Applications of Coupled Differential Equations, SIAM, Philadelphia, PA, USA, 2023, https://doi.org/10.1137/ 1.9781611977332.
- [81] R. H. GOODMAN, NLS bifurcations on the bowtie combinatorial graph and the dumbbell metric graph, Discrete Contin. Dyn. Syst., 39 (2019), pp. 2203–2232, https://doi.org/10.3934/dcds.2019093.
- [82] R. H. GOODMAN, G. CONTE, AND J. L. MARZUOLA, QGLAB: A MATLAB package for computations on quantum graphs, SIAM J. Sci. Comput., 47 (2025), pp. 428–453, https://doi.org/10.1137/ 23M1627729.
- [83] C. GRANELL, S. GÓMEZ, AND A. ARENAS, Dynamical interplay between awareness and epidemic spreading in multiplex networks, Phys. Rev. Lett., 111 (2013), 128701, https://doi.org/10.1103/PhysRevLett. 111.128701.
- [84] V. Grant, We thank Miss Mary Tsingou, 2020, https://web.archive.org/web/20240929141604/, https://discover.lanl.gov/publications/national-security-science/2020-winter/we-thank-miss-mary-tsingou/, last accessed 14 August 2023.
- [85] A. A. Gusev, Finite element mapping for spring network representations of the mechanics of solids, Phys. Rev. Lett., 93 (2004), 034302, https://doi.org/10.1103/PhysRevLett.93.034302.
- [86] T. HALILOGLU, I. BAHAR, AND B. ERMAN, Gaussian dynamics of folded proteins, Phys. Rev. Lett., 79 (1997), pp. 3090–3093, https://doi.org/10.1103/PhysRevLett.79.3090.
- [87] G. N. HASSOLD AND D. J. SROLOVITZ, Brittle fracture in materials with random defects, Phys. Rev. B, 39 (1989), pp. 9273–9281, https://doi.org/10.1103/PhysRevB.39.9273.
- [88] D. Helbing, Verkehrsdynamik: Neue Physikalische Modellierungskonzepte, Springer-Verlag, Heidelberg, Germany, 2013.
- [89] H. J. HERRMANN, B. DERRIDA, AND J. VANNIMENUS, Superconductivity exponents in two- and three-dimensional percolation, Phys. Rev. B, 30 (1984), pp. 4080–4082, https://doi.org/10.1103/PhysRevB. 30.4080.

- [90] H. J. HERRMANN, A. HANSEN, AND S. ROUX, Fracture of disordered, elastic lattices in two dimensions, Phys. Rev. B, 39 (1989), pp. 637–648, https://doi.org/10.1103/PhysRevB.39.637.
- [91] M. HOFMANN, J. B. KENNEDY, D. MUGNOLO, AND M. PLÜMER, Asymptotics and estimates for spectral minimal partitions of metric graphs, Integr. Equat. Oper. Theory, 93 (2021), 26, https://doi.org/ 10.1007/s00020-021-02635-7.
- [92] M. HOFMANN, J. B. KENNEDY, D. MUGNOLO, AND M. PLÜMER, On Pleijel's nodal domain theorem for quantum graphs, Ann. Henri Poincaré, 22 (2021), pp. 3841–3870, https://doi.org/10.1007/s00023-021-01077-6.
- [93] S. HOLDEN AND G. VASIL, A continuum limit for dense networks, preprint, arXiv:2301.07086, 2023.
- [94] A. Hrennikoff, Solution of problems of elasticity by the framework method, J. Appl. Mech., 8 (1941), pp. A169–A175, https://doi.org/10.1115/1.4009129.
- [95] O. Hul, S. Bauch, P. Pakoński, N. Savytskyy, K. Życzkowski, and L. Sirko, Experimental simulation of quantum graphs by microwave networks, Phys. Rev. E, 69 (2004), 056205, https://doi.org/10.1103/PhysRevE.69.056205.
- [96] V. Ježek and J. Lipovský, Application of quotient graph theory to three-edge star graphs, Acta Phys. Pol. A, 140 (2021), pp. 514–524, https://doi.org/10.12693/APhysPolA.140.514.
- [97] A. KAIRZHAN, D. E. PELINOVSKY, AND R. H. GOODMAN, Drift of spectrally stable shifted states on star graphs, SIAM J. Appl. Dyn. Syst., 18 (2019), pp. 1723–1755, https://doi.org/10.1137/19M1246146.
- [98] V. KALOSHIN, M. LEVI, AND M. SAPRYKINA, Arnol'd diffusion in a pendulum lattice, Comm. Pure Appl. Math., 67 (2014), pp. 748–775, https://doi.org/10.1002/cpa.21509.
- [99] Y. V. KARTASHOV, B. A. MALOMED, AND L. TORNER, Solitons in nonlinear lattices, Rev. Mod. Phys., 83 (2011), pp. 247–305, https://doi.org/10.1103/RevModPhys.83.247.
- [100] J. B. Kennedy, D. Mugnolo, and M. Täufer, Towards a theory of eigenvalue asymptotics on infinite metric graphs: The case of diagonal combs, preprint, arXiv:2403.10708, 2024.
- [101] S. KIRKPATRICK, Percolation and conduction, Rev. Mod. Phys., 45 (1973), pp. 574–588, https://doi.org/10.1103/RevModPhys.45.574.
- [102] V. Kostrykin and R. Schrader, Kirchhoff's rule for quantum wires, J. Phys. A, 32 (1999), pp. 595–630, https://doi.org/10.1088/0305-4470/32/4/006.
- [103] T. Kottos and U. Smilansky, Quantum chaos on graphs, Phys. Rev. Lett., 79 (1997), pp. 4794–4797, https://doi.org/10.1103/PhysRevLett.79.4794.
- [104] T. KOTTOS AND U. SMILANSKY, Periodic orbit theory and spectral statistics for quantum graphs, Ann. Phys., 274 (1999), pp. 76–124, https://doi.org/10.1006/aphy.1999.5904.
- [105] T. Kottos and U. Smilansky, Quantum graphs: A simple model for chaotic scattering, J. Phys. A, 36 (2003), pp. 3501–3524, https://doi.org/10.1088/0305-4470/36/12/337.
- [106] T. KOTWAL, F. MOSELEY, A. STEGMAIER, S. IMHOF, H. BRAND, T. KIESSLING, R. THOMALE, H. RONELLENFITSCH, AND J. DUNKEL, Active topolectrical circuits, Proc. Natl. Acad. Sci. USA, 118 (2021), e2106411118, https://doi.org/10.1073/pnas.2106411118.
- [107] M. KOVÁCS AND M. VÁGHY, Neumann-Neumann type domain decomposition of elliptic problems on metric graphs, BIT Numer. Math., 65 (2025), 27, https://doi.org/10.1007/s10543-025-01067-8.
- [108] H. KRAVITZ, M. BRIO, AND J.-G. CAPUTO, Localized eigenvectors on metric graphs, Math. Comput. Simul., 214 (2023), pp. 352–372, https://doi.org/10.1016/j.matcom.2023.07.011.
- [109] H. KRAVITZ, C. DURÓN, AND M. BRIO, A coupled spatial-network model: A mathematical framework for applications in epidemiology, Bull. Math. Biol., 86 (2024), 132, https://doi.org/10.1007/s11538-024-01364-3.
- [110] P. Kuchment, Graph models for waves in thin structures, Waves Random Media, 12 (2002), pp. R1–R24, https://doi.org/10.1088/0959-7174/12/4/201.
- [111] P. KUCHMENT, Quantum graphs: I. Some basic structures, Waves Random Media, 14 (2003), pp. S107–S128, https://doi.org/10.1088/0959-7174/14/1/014.
- [112] P. KUCHMENT, Quantum graphs: II. Some spectral properties of quantum and combinatorial graphs, J. Phys. A, 38 (2005), pp. 4887–4900, https://doi.org/10.1088/0305-4470/38/22/013.
- [113] Y. Kuramoto, Self-entrainment of a population of coupled non-linear oscillators, in International Symposium on Mathematical Problems in Theoretical Physics, Springer-Verlag, Heidelberg, Germany, 1975, pp. 420–422, https://doi.org/10.1007/BFb0013365.

- [114] P. Kurasov, Understanding quantum graphs, Acta Phys. Pol., 136 (2019), pp. 797–802, https://doi.org/ 10.12693/APhysPolA.136.797.
- [115] P. Kurasov, Spectral Geometry of Graphs, Oper. Theory Adv. Appl. 293, Birkhäuser, Berlin, Germany, 2024.
- [116] J. E. LAGNESE, G. LEUGERING, AND E. J. P. G. SCHMIDT, Modelling of dynamic networks of thin thermoelastic beams, Math. Methods Appl. Sci., 16 (1993), pp. 327–358, https://doi.org/10.1002/ mma.1670160503.
- [117] M. LAWNICZAK, P. KURASOV, S. BAUCH, M. BIALOUS, A. AKHSHANI, AND L. SIRKO, A new spectral invariant for quantum graphs, Sci. Rep., 11 (2021), 15342, https://doi.org/10.1038/s41598-021-94331-0.
- [118] M. ŁAWNICZAK, J. LIPOVSKÝ, AND L. SIRKO, Non-Weyl microwave graphs, Phys. Rev. Lett., 122 (2019), 140503, https://doi.org/10.1103/PhysRevLett.122.140503.
- [119] T. LAWRIE, T. STARKEY, G. TANNER, D. MOORE, P. SAVAGE, AND G. CHAPLAIN, Application of quantum graph theory to metamaterial design: Negative refraction of acoustic waveguide modes, Phys. Rev. Mater., 8 (2024), 105201, https://doi.org/10.1103/PhysRevMaterials.8.105201.
- [120] T. LAWRIE, G. TANNER, AND G. J. CHAPLAIN, Engineering metamaterial interface scattering coefficients via quantum graph theory, Acta Phys. Pol., 144 (2023), pp. 486–494, https://doi.org/10.12693/ APhysPolA.144.486.
- [121] T. LAWRIE, G. TANNER, AND D. CHRONOPOULOS, A quantum graph approach to metamaterial design, Sci. Rep., 12 (2022), 18006, https://doi.org/10.1038/s41598-022-22265-2.
- [122] Z. LI, M. A. PORTER, AND B. CHOUBEY, Recurrence recovery in heterogeneous Fermi-Pasta-Ulam-Tsingou systems, Chaos, 33 (2023), 093108, https://doi.org/10.1063/5.0154970.
- [123] J. Lu, J. Che, X. Zhang, and B. Dietz, Experimental and numerical investigation of parametric spectral properties of quantum graphs with unitary or symplectic symmetry, Phys. Rev. E, 102 (2020), 022309, https://doi.org/10.1103/PhysRevE.102.022309.
- [124] G. Lumer, Équations de diffusion sur des réseaux infinis, in Séminaire Goulaouic-Schwartz (École polytechnique), 1979–1980, Talk no. 18.
- [125] G. LUMER, Connecting of local operators and evolution equations on networks, in Potential Theory, Copenhagen 1979 (Proc. Colloq., Copenhagen, 1979), F. Hirsch, ed., Springer-Verlag, Heidelberg, Germany, 1980, pp. 230–243, https://doi.org/10.1007/BFb0086338.
- [126] B. MALOMED, Nonlinear Schrödinger equations, in Encyclopedia of Nonlinear Science, A. Scott, ed., Routledge, London, UK, 2006, pp. 639–643, https://doi.org/10.4324/9780203647417.
- [127] J. L. MARZUOLA AND D. E. PELINOVSKY, Ground state on the dumbbell graph, Appl. Math. Res. eXpress, 2016 (2016), pp. 98–145, https://doi.org/10.1093/amrx/abv011.
- [128] H. MASOOMY, T. CHOU, AND L. BÖTTCHER, Impact of random and targeted disruptions on information diffusion during outbreaks, Chaos, 33 (2023), 033145, https://doi.org/10.1063/5.0139844.
- [129] N. MASUDA, M. A. PORTER, AND R. LAMBIOTTE, Random walks and diffusion on networks, Phys. Rep., 716–717 (2017), pp. 1–58, https://doi.org/10.1016/j.physrep.2017.07.007.
- [130] H. V. McIntosh, On accidental degeneracy in classical and quantum mechanics, Amer. J. Phys., 27 (1959), pp. 620–625, https://doi.org/10.1119/1.1934944.
- [131] G. S. MEDVEDEV AND D. E. PELINOVSKY, Turing bifurcation in the Swift-Hohenberg equation on deterministic and random graphs, J. Nonlinear Sci., 34 (2024), 88, https://doi.org/10.1007/s00332-024-10054-2.
- [132] V. MEHANDIRATTA, M. MEHRA, AND G. LEUGERING, Optimal control problems driven by time-fractional diffusion equations on metric graphs: Optimality system and finite difference approximation, SIAM J. Control Optim., 59 (2021), pp. 4216-4242, https://doi.org/10.1137/20M1340332.
- [133] D. MERCIER AND V. RÉGNIER, Spectrum of a network of Euler-Bernoulli beams, J. Math. Anal. Appl., 337 (2008), pp. 174–196, https://doi.org/10.1016/j.jmaa.2007.03.080.
- [134] P. MINDT, J. LANG, AND P. DOMSCHKE, Entropy-preserving coupling of hierarchical gas models, SIAM J. Math. Anal., 51 (2019), pp. 4754–4775, https://doi.org/10.1137/19M1240034.
- [135] E. Mones, N. A. M. Araújo, T. Vicsek, and H. J. Herrmann, Shock waves on complex networks, Sci. Rep., 4 (2014), 4949, https://doi.org/10.1038/srep04949.

- [136] A. MURANOVA, On the notion of effective impedance, Oper. Matrices, 14 (2020), pp. 723-741, https://doi.org/10.7153/oam-2020-14-46.
- [137] A. Muranova, Effective impedance over ordered fields, J. Math. Phys., 62 (2021), 033502, https://doi.org/10.1063/5.0007130.
- [138] A. Muranova, On the effective impedance of finite and infinite networks, Potential Anal., 56 (2022), pp. 697–721, https://doi.org/10.1007/s11118-021-09901-8.
- [139] A. MURANOVA AND R. SCHIPPA, Eigenvalues of the normalized complex Laplacian on finite electrical networks, preprint, arXiv:2012.12759, 2020.
- [140] A. MURANOVA AND W. Woess, Networks with complex weights: Green function and power series, Mathematics, 10 (2022), 820, https://doi.org/10.3390/math10050820.
- [141] S. NAUER, L. BÖTTCHER, AND M. A. PORTER, Random-graph models and characterization of granular networks, J. Complex Networks, 8 (2020), cnz037, https://doi.org/10.1093/comnet/cnz037.
- [142] A. Nealen, M. Müller, R. Keiser, E. Boxerman, and M. Carlson, Physically based deformable models in computer graphics, Computer Graphics Forum, 25 (2006), pp. 809–836, https://doi.org/ 10.1111/j.1467-8659.2006.01000.x.
- [143] M. E. J. NEWMAN, Networks, 2nd ed., Oxford University Press, Oxford, UK, 2018.
- [144] D. Noja, Nonlinear Schrödinger equation on graphs: Recent results and open problems, Philos. Trans. Roy. Soc. A: Math. Phys. Eng. Sci., 372 (2014), 20130002, https://doi.org/10.1098/rsta.2013.0002.
- [145] J. NOKKALA, J. PIILO, AND G. BIANCONI, Complex quantum networks: A topical review, J. Phys. A, 57 (2024), 233001, https://doi.org/10.1088/1751-8121/ad41a6.
- [146] A. Nussbaum, Group theory and normal modes, Amer. J. Phys., 36 (1968), pp. 529–539, https://doi. org/10.1119/1.1974965.
- [147] E. K. Oldaker (Née Swindle), Spectral Properties of Quantum Graphs with Symmetry, Ph.D. thesis, Baylor University, 2019, https://baylor-ir.tdl.org/items/ea6f5612-3859-49ca-a6a3-dd8a29581cb5.
- [148] L. Papadopoulos, M. A. Porter, K. E. Daniels, and D. S. Bassett, Network analysis of particles and grains, J. Complex Networks, 6 (2018), pp. 485–565, https://doi.org/10.1093/comnet/cny005.
- [149] R. PASTOR-SATORRAS, C. CASTELLANO, P. VAN MIEGHEM, AND A. VESPIGNANI, Epidemic processes in complex networks, Rev. Mod. Phys., 87 (2015), pp. 925–979, https://doi.org/10.1103/RevModPhys. 87.925.
- [150] C. R. Paul, Analysis of Multiconductor Transmission Lines, John Wiley & Sons, Hoboken, NJ, USA, 2007
- [151] B. PICCOLI AND M. GARAVELLO, *Traffic Flow on Networks*, American Institute of Mathematical Sciences, Pasadena, CA, USA, 2006.
- [152] L. PITAEVSKII AND S. STRINGARI, Bose-Einstein Condensation and Superfluidity, Oxford University Press, Oxford, UK, 2016.
- [153] M. A. PORTER, Nonlinearity + networks: A 2020 vision, in Emerging Frontiers in Nonlinear Science, P. G. Kevrekidis, J. Cuevas-Maraver, and A. Saxena, eds., Springer International Publishing, Cham, Switzerland, 2020, pp. 131–159, https://doi.org/10.1007/978-3-030-44992-6_6.
- [154] M. A. PORTER AND J. P. GLEESON, Dynamical Systems on Networks: A Tutorial, Front. Appl. Dyn. Syst. Rev. Tutor. 4, Springer International Publishing, Cham, Switzerland, 2016, https://doi.org/ 10.1007/978-3-319-26641-1.
- [155] M. POURNAJAR, M. ZAISER, AND P. MORETTI, Edge betweenness centrality as a failure predictor in network models of structurally disordered materials, Sci. Rep., 12 (2022), 11814, https://doi.org/10.1038/ s41598-022-15842-v.
- [156] F. A. RODRIGUES, T. K. DM. PERON, P. JI, AND J. KURTHS, The Kuramoto model in complex networks, Phys. Rep., 610 (2016), pp. 1–98, https://doi.org/10.1016/j.physrep.2015.10.008.
- [157] K. RUEDENBERG AND C. W. SCHERR, Free-electron network model for conjugated systems. I. Theory, J. Chem. Phys., 21 (1953), pp. 1565–1581, https://doi.org/10.1063/1.1699299.
- [158] K. K. Sabirov, D. B. Babajanov, D. U. Matrasulov, and P. G. Kevrekidis, Dynamics of Dirac solitons in networks, J. Phys. A, 51 (2018), 435203, https://doi.org/10.1088/1751-8121/aadfb0.
- [159] G. Salerno, A. Berardo, T. Ozawa, H. M. Price, L. Taxis, N. M. Pugno, and I. Carusotto, Spin-orbit coupling in a hexagonal ring of pendula, New J. Phys., 19 (2017), 055001, https://doi.org/ 10.1088/1367-2630/aa6c03.

- [160] G. SALERNO, T. OZAWA, H. M. PRICE, AND I. CARUSOTTO, Floquet topological system based on frequency-modulated classical coupled harmonic oscillators, Phys. Rev. B, 93 (2016), 085105, https://doi.org/10.1103/PhysRevB.93.085105.
- [161] T. Schneider, O. R. Dunbar, J. Wu, L. Böttcher, D. Burov, A. Garbuno-Inigo, G. L. Wagner, S. Pei, C. Daraio, R. Ferrari, and J. Shaman, Epidemic management and control through risk-dependent individual contact interventions, PLOS Comput. Biol., 18 (2022), e1010171, https://doi.org/10.1371/journal.pcbi.1010171.
- [162] C. Sintavanuruk, Y. Mori, R. Farhadifar, and E. Katifori, Self-construction and destruction of living transport networks, preprint, arXiv:2503.20532, 2025.
- [163] Z. Sobirov, D. Babajanov, D. Matrasulov, K. Nakamura, and H. Uecker, Sine-Gordon solitons in networks: Scattering and transmission at vertices, Europhys. Lett., 115 (2016), 50002, https://doi.org/10.1209/0295-5075/115/50002.
- [164] M. STOLL AND M. WINKLER, Optimization of a partial differential equation on a complex network, preprint, arXiv:1907.07806, 2019.
- [165] G. Strang, The discrete cosine transform, SIAM Rev., 41 (1999), pp. 135–147, https://doi.org/ 10.1137/S0036144598336745.
- [166] S. H. Strub and L. Böttcher, Modeling deformed transmission lines for continuous strain sensing applications, Meas. Sci. Technol., 31 (2019), 035109, https://doi.org/10.1088/1361-6501/ab5389.
- [167] T. STUYCK, Cloth Simulation for Computer Graphics, Synthesis Lectures on Visual Computing, Morgan & Claypool Publishers, San Rafael, CA, USA, 2018.
- [168] R. SÜSSTRUNK AND S. D. HUBER, Observation of phononic helical edge states in a mechanical topological insulator, Science, 349 (2015), pp. 47–50, https://doi.org/10.1126/science.aab0239.
- [169] G. TESCHL, Jacobi Operators and Completely Integrable Nonlinear Lattices, American Mathematical Society, Providence, RI, USA, 2000.
- [170] Y. Tian and L. Wang, Dynamics of opinion formation, social power evolution, and naïve learning in social networks, Annu. Rev. Control, 55 (2023), pp. 182–193, https://doi.org/10.1016/j.arcontrol. 2023.04.001.
- [171] M. Toda, Vibration of a chain with nonlinear interaction, J. Phys. Soc. Jpn., 22 (1967), pp. 431–436, https://doi.org/10.1143/JPSJ.22.431.
- [172] M. Toda, Development of the theory of a nonlinear lattice, Prog. Theor. Phys. Supp., 59 (1976), pp. 1–35, https://doi.org/10.1143/PTPS.59.1.
- [173] M. Toda, Theory of Nonlinear Lattices, Springer-Verlag, Heidelberg, Germany, 2012.
- [174] M. WALLACE, R. FERES, AND G. YABLONSKY, Reaction-diffusion on metric graphs: From 3D to 1D, Comput. Math. Appl., 73 (2017), pp. 2035–2052, https://doi.org/10.1016/j.camwa.2017.02.033.
- [175] H. Weyl, The Theory of Groups and Quantum Mechanics, Courier Corporation, Chelmsford, MA, USA, 1950.
- [176] B. XIA, The Ablowitz-Ladik system on a graph, Nonlinearity, 32 (2019), pp. 4729–4761, https://doi.org/10.1088/1361-6544/ab36f2.
- [177] M. XIA, L. BÖTTCHER, AND T. CHOU, Controlling epidemics through optimal allocation of test kits and vaccine doses across networks, IEEE Trans. Network Sci. Eng., 9 (2022), pp. 1422–1436, https://doi.org/10.1109/TNSE.2022.3144624.
- [178] M. XIA, L. BÖTTCHER, AND T. CHOU, Spectrally adapted physics-informed neural networks for solving unbounded domain problems, Mach. Learn.: Sci. Technol., 4 (2023), 025024, https://doi.org/10.1088/2632-2153/acd0a1.
- [179] J. G. Zabolitzky, Monte Carlo evidence against the Alexander-Orbach conjecture for percolation conductivity, Phys. Rev. B, 30 (1984), pp. 4077-4079, https://doi.org/10.1103/PhysRevB.30.4077.
- [180] A. Zee, Group Theory in a Nutshell for Physicists, Princeton University Press, Princeton, NJ, USA, 2016.
- [181] W. Zhang, X. Zhang, J. Che, J. Lu, M. Miski-Oglu, and B. Dietz, Experimental study of closed and open microwave waveguide graphs with preserved and partially violated time-reversal invariance, Phys. Rev. E, 106 (2022), 044209, https://doi.org/10.1103/PhysRevE.106.044209.
- [182] N. F. ZORN AND J. ZAUMSEIL, Charge transport in semiconducting carbon nanotube networks, Appl. Phys. Rev., 8 (2021), 041318, https://doi.org/10.1063/5.0065730.